$G\alpha_{11}$ mutation in mice causes hypocalcemia rectifiable by calcilytic therapy

Caroline M. Gorvin[1], Fadil M. Hannan[1,2], Sarah A. Howles[1], Valerie N. Babinsky[1], Sian E. Piret[1], Angela Rogers[1], Andrew J. Freidin[3], Michelle Stewart[4], Anju Paudyal[4], Tertius A. Hough[4], M. Andrew Nesbit[1,5], Sara Wells[4], Tonia L. Vincent[3], Stephen D. M. Brown[4], Roger D. Cox[4], Rajesh V. Thakker[1]

Authorship note: Caroline Gorvin, Fadil Hannan and Sarah Howles contributed equally to this work

[1]Academic Endocrine Unit, Radcliffe Department of Medicine, University of Oxford, Oxford, UK. [2]Department of Musculoskeletal Biology, Institute of Ageing and Chronic Disease, University of Liverpool, Liverpool, UK. [3]ARUK Centre for Osteoarthritis Pathogenesis, The Kennedy Institute of Rheumatology, University of Oxford, Oxford, UK. [4]MRC Mammalian Genetics Unit and Mary Lyon Centre, MRC Harwell Institute, Harwell Science and Innovation Campus, UK. [5]Biomedical Sciences Research Institute, Ulster University, Coleraine, UK.

Address correspondence to: Rajesh V. Thakker at the Academic Endocrine Unit, Radcliffe Department of Medicine, Oxford Centre for Diabetes, Endocrinology and Metabolism (OCDEM), Churchill Hospital, Oxford OX3 7LJ, United Kingdom. Tel no: 01865 857501. Fax no: 01865 875502. Email: rajesh.thakker@ndm.ox.ac.uk.

Conflict of interest: The authors have declared that no conflict of interest exists.

Manuscript word count = 9540 (including tables and legends) (limit =12000 words)

Abstract

Heterozygous germline gain-of-function mutations of G-protein subunit α_{11} ($G\alpha_{11}$), a signaling partner for the calcium-sensing receptor (CaSR), result in autosomal dominant hypocalcemia type 2 (ADH2). ADH2 may cause symptomatic hypocalcemia with low circulating parathyroid hormone (PTH) concentrations. Effective therapies for ADH2 are currently not available and a mouse model for ADH2 would help in assessment of potential therapies. We hypothesised that a previously reported dark skin mouse mutant (*Dsk7*), which has a germline hypermorphic $G\alpha_{11}$ mutation, Ile62Val, may be a model for ADH2 and allow evaluation of calcilytics, which are CaSR negative allosteric modulators, as a targeted therapy for this disorder. Mutant *Dsk7/+* and *Dsk7/Dsk7* mice were shown to have hypocalcemia and reduced plasma PTH concentrations, similar to ADH2 patients. *In vitro* studies showed the mutant Val62 $G\alpha_{11}$ to up-regulate CaSR-mediated intracellular calcium and MAPK signaling, consistent with a gain-of-function. Treatment with NPS-2143, a calcilytic compound, normalised these signaling responses. *In vivo,* NPS-2143 induced a rapid and marked rise in plasma PTH and calcium concentrations in *Dsk7/Dsk7* and *Dsk7/+* mice, which became normocalcemic. Thus, these studies have established *Dsk7* mice, which harbor a germline gain-of-function $G\alpha_{11}$ mutation, as a model for ADH2; and demonstrated calcilytics as a potential targeted therapy.

Introduction

Autosomal dominant hypocalcemia (ADH) is a disorder of systemic calcium homeostasis caused by increased sensitivity of the calcium-sensing receptor (CaSR) signaling pathway to extracellular calcium (Ca^{2+}_o) concentrations (1, 2). The CaSR is a widely expressed class C G-protein coupled receptor (GPCR) that plays a pivotal role in Ca^{2+}_o homeostasis by transducing elevations in the prevailing Ca^{2+}_o concentration into multiple signaling cascades that include $G_{q/11}$-protein mediated activation of phospholipase C (PLC), which in the parathyroid glands induce increases in intracellular calcium (Ca^{2+}_i) and mitogen-activated protein kinase (MAPK) signaling responses that lead to decreased parathyroid hormone (PTH) secretion (3). ADH is associated with hypocalcemia, hyperphosphatemia, hypomagnesemia, inappropriately low or normal PTH concentrations, and some patients may also be hypercalciuric (1, 4), or develop a Bartter-like syndrome characterised by hypokalemic alkalosis, renal salt wasting and hyperreninemic hyperaldosteronism (5, 6). Approximately 50% of patients develop symptomatic hypocalcemia, and >35% have ectopic calcifications within the kidneys and basal ganglia (1, 2, 7, 8). ADH is a genetically heterogeneous disorder comprised of two variants, which are known as ADH type 1 (ADH1) and ADH type 2 (ADH2). ADH1 (OMIM #601198) is caused by germline mutations of the CaSR, which is encoded by the *CASR* gene on chromosome 3q21.1 (1, 9); whereas, ADH2 (OMIM #615361) is caused by germline mutations of the widely expressed G-protein subunit α_{11} ($G\alpha_{11}$) protein, which is encoded by the *GNA11* gene on chromosome 19p13.3 (2, 7, 8, 10). Both CaSR and $G\alpha_{11}$ mutations identified in ADH patients have been demonstrated to enhance CaSR-mediated Ca^{2+}_i and MAPK signaling in cellular studies, consistent with a gain-of-function (1, 2, 7, 9-11).

Mouse models with gain-of-function *Casr* mutations have been generated by chemical mutagenesis and knock-in strategies, and shown to have a phenotype closely resembling ADH1 in humans, with hypocalcemia, hyperphosphatemia, reduced PTH concentrations, hypercalciuria and ectopic calcifications (12, 13). Such models have been utilized to evaluate calcilytic compounds, which are negative allosteric CaSR modulators that represent a potential targeted therapy for ADH

(14-17). Indeed, a long-acting amino-alcohol calcilytic compound known as NPS-2143 has been shown *in vivo* to rectify the hypocalcemia of *Nuf* mice, which harbor a germline gain-of-function *Casr* mutation, Leu723Gln (13, 18). Recent *in vitro* studies have also revealed NPS-2143 to normalise the gain-of-function caused by $G\alpha_{11}$ mutations that lead to ADH2 (11). However, it remains unclear whether this calcilytic may rectify the hypocalcemia associated with ADH2, and mouse models that harbor *Gna11* mutations in association with hypocalcemia have not been reported to be available for such *in vivo* studies. Such mouse models would also aid the further phenotypic characterization of ADH2, as limited information is available from the small numbers of patients studied to date (2, 7, 8, 10, 19).

To develop a mouse model for ADH2, we conducted studies to investigate the calcitropic phenotype of a previously reported mouse mutant known as *Gna11*^{Mhdadsk7} or "dark skin 7", and henceforth referred to as *Dsk7*, which has increased dermal pigmentation in association with a germline hypermorphic *Gna11* mutation, Ile62Val (formerly referred to as Ile63Val) (20). We hypothesised that *Dsk7* mice would exhibit dysregulation of Ca^{2+}_{o} homeostasis in keeping with ADH2. Our study has revealed *Dsk7* mice to have hypocalcemia and reduced PTH concentrations, which are caused by a gain-of-function *Gna11* mutation that leads to upregulation of CaSR-mediated Ca^{2+}_{i} and MAPK signaling responses. Moreover, we demonstrate that NPS-2143 treatment rectifies this gain-of-function *in vitro* and ameliorates the hypocalcemia of *Dsk7* mice.

Results

Genotype and phenotype studies of Dsk7 mice. DNA sequence analysis of *Gna11* in *Dsk7* mice confirmed the reported A-to-G transition (c.184A>G, RefSeq Accession NM_002067.4) at codon 62 of the $G\alpha_{11}$ protein resulting in an Ile to Val missense substitution (Supplementary Figure 1A-B) (20). This mutation also led to the loss of a *FokI* restriction endonuclease site (Supplementary Figure 1B), as reported (20), which was used to confirm the presence of the mutation in *Dsk7* mice (Supplementary Figure 1C-D), and for genotyping of subsequent generations. Analysis of offspring bred from crosses of *Dsk7/+* x *Dsk7/+* mice showed that the proportion bred as homozygous-affected *Dsk7/Dsk7* mice were >30% less (x^2 =10.20, df = 2, P < 0.01) than would be expected from a Mendelian pattern of inheritance (Supplementary Table 1). The *Dsk7/Dsk7* mice also had significantly reduced body weight and increased skin pigmentation (data not shown), when compared to age-matched WT (+/+) mice (Table 1), as previously reported (20).

Biochemical analysis of plasma samples collected under isoflurane terminal anesthesia revealed male and female *Dsk7/+* and *Dsk7/Dsk7* mice to be significantly hypocalcemic and hyperphosphatemic, and to have significantly reduced PTH concentrations when compared to +/+ mice (Figure 1, Table 1). The hypocalcemia was significantly more marked in *Dsk7/Dsk7* mice compared to heterozygous-affected *Dsk7/+* mice (Figure 1, Table 1). Reduced FGF-23 concentrations were noted in *Dsk7/Dsk7* mice compared to +/+ mice (Table 1). No significant differences were observed in plasma urea and creatinine concentrations, alkaline phosphatase activity or 1,25-dihydroxyvitamin D concentrations (Table 1). Twenty-four hour urinary calcium excretion and urinary calcium/creatinine ratios were significantly reduced in female *Dsk/+* mice, although fractional excretion of calcium was not different between either male or female *Dsk7* mice and respective +/+ mice (Table 2). The tubular maximum reabsorption of phosphate was significantly increased in *Dsk7/+* and *Dsk7/Dsk7* mice (Table 2), consistent with the low circulating PTH concentrations of these mice (Figure 1, Table 1) (21). Fractional excretion of sodium and potassium were not altered (Table 2). Whole body dual-energy X-ray absorptiometry (DXA) showed no differences in bone mineral density (BMD) between male and female *Dsk7* mice and respective +/+ mice (Table 3).

Micro-CT analysis of trabecular bone also showed no alterations in the bone volume fraction, or in the thickness or number of trabeculae between male or female *Dsk7* mice and respective +/+ mice (Table 3). Ophthalmological examination did not reveal any lens opacifications in *Dsk7/Dsk7* mice (data not shown), and these findings contrast with *Nuf* mice, which harbor a gain-of-function *Casr* mutation in association with hypocalcemia and cataracts (18).

Effects of Ile62Val $G\alpha_{11}$ mutation on $G\alpha_{11}$ structure and CaSR-mediated signaling. The Ile62 residue is located within the α1 helix of the GTPase domain of $G\alpha_{11}$, and close to the Arg60 residue, which has been reported to be mutated in ADH2 patients (Figure 2A) (7, 8). The WT Ile62 residue, which is encoded in exon 2 of the *Gna11* gene (Figure 2A), is absolutely conserved in $G\alpha_{11}$ orthologs and highly conserved in Gα-subunit paralogs (Figure 2B). To determine the importance of the WT Ile62 residue for $G\alpha_{11}$ function, homology modeling was undertaken using the crystal structure of the related $G\alpha_q$ and $G\alpha_i$ proteins (22, 23). This revealed the WT Ile62 residue to be located at the interface between the Gα-subunit helical and GTPase domains (Figure 2C), and to comprise part of a conserved hydrophobic cluster of amino acid residues within the GTPase domain of the Gα-subunit, which play a key role in stabilizing G-proteins in an inactive GDP-bound conformation (Figure 2D) (23). These findings predicted that mutation of the conserved WT Ile62 $G\alpha_{11}$ residue to a mutant Val62 residue would destabilize the inactive GDP-bound Gα-subunit, thereby leading to guanine-nucleotide exchange and $G\alpha_{11}$ activation (23).

To determine the effects of these predicted changes in $G\alpha_{11}$ structure on CaSR-mediated signaling, HEK293 cells stably expressing the CaSR (HEK-CaSR) were transiently transfected with pBI-CMV2-*GNA11* constructs expressing either the WT (Ile62) or mutant (Val62) $G\alpha_{11}$ proteins. This bidirectional pBI-CMV2 vector allows for co-expression of $G\alpha_{11}$ and GFP at equivalent levels (2); and expression of the CaSR, $G\alpha_{11}$ and GFP was confirmed by fluorescence microscopy and/or Western blot analyses (Figure 3A-B). The expression of $G\alpha_{11}$ was shown to be similar in cells transiently transfected with WT or mutant proteins, and greater than that observed in untransfected cells (Supplementary Figure 2). The expression of mutant $G\alpha_{11}$ in transfected cells together with that of the endogenous expression of WT $G\alpha_{11}$ corresponds to the heterozygous situation *in vivo* (Figure

3B and Supplementary Figure 2). The responses of Ca^{2+}_i to alterations in $[Ca^{2+}]_o$ of cells expressing the different *GNA11* vectors were assessed by flow cytometry. The Ca^{2+}_i responses in WT and mutant $G\alpha_{11}$-expressing cells were shown to increase in a dose-dependent manner following stimulation with increasing concentrations of Ca^{2+}_o. However, responses in mutant Val62 expressing cells were significantly elevated compared to WT expressing cells (Figure 3C). Thus, the Val62 mutant-expressing cells showed a leftward shift in the concentration-response curve (Figure 3C), with significantly reduced mean half-maximal response (EC_{50}) value ($P < 0.001$, n=7) of 2.57 mM (95% confidence interval (CI) 2.47-2.67 mM) for Val62 expressing cells, compared to 3.02 mM (95% CI 2.93-3.10 mM) for WT expressing cells (Figure 3D), consistent with a gain-of-function of the $G\alpha_{11}$ mutant, as observed with $G\alpha_{11}$ mutations that lead to ADH2 (2, 7, 10, 11). The Val62 $G\alpha_{11}$ mutant did not alter the maximal Ca^{2+}_i signaling responses (Figure 3E), but was associated with a significant reduction of the Hill coefficient ($P < 0.01$) (Figure 3F).

In vitro effects of NPS-2143 treatment on Ca^{2+}_i and MAPK responses of the Val62 $G\alpha_{11}$ mutant. To investigate whether allosteric inhibition of the CaSR can rectify the gain-of-function associated with the Ile62Val $G\alpha_{11}$ mutation, NPS-2143 was added at 20 and 40 nM concentrations, as similar doses of this calcilytic have been reported to rectify the altered signaling responses associated with ADH2-causing $G\alpha_{11}$ mutations (11). An assessment of Ca^{2+}_i responses showed 20 nM NPS-2143 to increase the EC_{50} of Val62-expressing mutant cells to 2.97 mM (95% CI 2.88-3.08 mM), so that this was not significantly different from the EC_{50} of untreated WT cells (Figure 3C-D). However, addition of NPS-2143 at the higher 40 nM dose increased the EC_{50} of mutant cells to a value of 3.48 mM (95% CI 3.42-3.55 mM), which was significantly greater than that of untreated WT cells ($P < 0.01$) (Figure 3C-D). NPS-2143 had no effect on the maximal responses or Hill coefficients of mutant-expressing cells (Figure 3E-F).

Some gain-of-function $G\alpha_{11}$ mutations have been reported to promote tumorigenesis by constitutively upregulating MAPK signaling (24), and we therefore assessed the oncogenic potential of the Ile62Val $G\alpha_{11}$ mutation in HEK-CaSR cells by measurements of phosphorylated ERK (pERK), which is a key component of the MAPK cascade (7, 25). WT and mutant pBI-CMV2-*GNA11* vectors

were transiently transfected into HEK-CaSR cells and the fold-change increase in pERK proteins were measured following exposure to varying $[Ca^{2+}]_o$. Western blot analysis confirmed expression of WT and mutant $G\alpha_{11}$ proteins in cells used for the pERK experiments (Figure 4A). In the absence of $Ca^{2+}{}_o$ stimulation, the basal pERK responses of the Val62 mutant were not significantly different from cells expressing WT $G\alpha_{11}$ (Figure 4B), whereas exposure to $Ca^{2+}{}_o$ led to significantly increased pERK fold-change responses of cells expressing the Val62 $G\alpha_{11}$ mutant (Val62 = 9.4±1.4) when compared to cells expressing WT $G\alpha_{11}$ (Ile62 = 4.1±0.5, $P < 0.01$) (Figure 4B). NPS-2143 was next added to cells expressing the Val62 $G\alpha_{11}$ mutant protein (Figure 4C), and which had been stimulated with 10 mM $Ca^{2+}{}_o$. Exposure to 20 nM of this calcilytic compound normalized the elevated pERK responses (Figure 4D). The effect of the Val62 $G\alpha_{11}$ mutant on MAPK signaling was also investigated by measuring gene transcription induced by a serum-response element (SRE) containing luciferase reporter construct, which is a downstream mediator of ERK signaling (7, 25). Western blot analysis confirmed expression of WT and mutant $G\alpha_{11}$ proteins in cells used for the SRE reporter experiments (Figure 4E). In the absence of $Ca^{2+}{}_o$ stimulation, the basal SRE reporter activity of the Val62 mutant was not significantly different from cells expressing WT $G\alpha_{11}$ (Figure 4F), whereas $Ca^{2+}{}_o$ stimulation led to significantly increased SRE reporter fold-change responses of cells expressing the Val62 $G\alpha_{11}$ mutant (Val62 = 20.7±1.5 compared to 11.0±0.4 for the Ile62 WT $G\alpha_{11}$, $P < 0.05$) (Figure 4F). NPS-2143 was then added at a dose of 20 nM to cells expressing the Val62 $G\alpha_{11}$ mutant protein (Figure 4G), in the presence of 10 mM $Ca^{2+}{}_o$, and this normalized the increased SRE reporter responses (Figure 4H).

In vivo effects of NPS-2143 on the hypocalcemia of Dsk7 mice. We next assessed whether the hypocalcemia of *Dsk7* mice may be improved by treatment with NPS-2143. Previous studies have demonstrated that i.p. administration of a 30 mg/kg NPS-2143 dose significantly increases plasma calcium and PTH concentrations in *Nuf* mice with a gain-of-function *Casr* mutation, but is associated with adverse effects on renal function (13). In contrast, a study using oral gavage administration of NPS-2143 in WT rats has reported that a dose of 100 μmol/kg can increase PTH responses without adverse renal effects (26). We therefore evaluated the effects of i.p. and oral gavage administration of

NPS-2143 in +/+ mice, and showed that a single oral gavage 100 μmol/kg dose of NPS-2143 significantly increased plasma calcium without altering renal function, whereas i.p. injection of this calcilytic led to a significant rise in plasma urea and creatinine (Supplementary Figure 2). We therefore administered a 100 μmol/kg bolus of NPS-2143 by oral gavage to +/+, *Dsk7/+* and *Dsk7/Dsk7* mice and measured PTH, calcium, phosphate, urea and creatinine concentrations at 0, 1, 2, 6 and 24h post-dose using plasma samples obtained from the lateral tail vein following application of topical local anesthesia. Administration of NPS-2143 led to a 4-5-fold elevation in plasma PTH concentrations in +/+, *Dsk7/+* and *Dsk7/Dsk7* mice, with a maximal rise in PTH occurring at 1-2h post-dose (Figure 5A-C). The rise in PTH was associated with a significant increase in plasma calcium concentrations in +/+, *Dsk7/+,* and *Dsk7/Dsk7* mice, which were maximally elevated (0.25-0.5 mmol/L above baseline values) at 2h post-dose (Figure 5D-F). Indeed, administration of 100 μmol/kg NPS-2143 normalised the plasma calcium concentrations of *Dsk7/Dsk7* mice, whereas *Dsk7/+* mice became transiently hypercalcemic (Figure 5D-F). NPS-2143 treatment also led to a transient rise in plasma phosphate concentrations in +/+ and *Dsk7/Dsk7* mice (Figure 5G-I), which was not associated with any increases in plasma urea or creatinine (Supplementary Figure 3). Thus, these studies demonstrate that a single dose of NPS-2143 can rectify the hypocalcemia of *Dsk7/+* and *Dsk7/Dsk7* mice.

Discussion

Our studies have demonstrated that *Dsk7* mice, which harbor a germline Ile62Val *Gna11* mutation (24), are hypocalcemic, hyperphosphatemic and have reduced circulating PTH concentrations. Thus, *Dsk7* mice represent a mouse model for the human disorder of ADH2, which is caused by gain-of-function *GNA11* mutations (2, 7, 8, 10). In support of this, the Ile62Val $G\alpha_{11}$ mutant protein enhanced the signaling responses of CaSR-expressing cells *in vitro*, and this data indicates that the *Gna11* mutation is leading to the observed phenotype in *Dsk7* mice. The Ile62Val *Gna11* mutation showed a gene dosage effect with the heterozygous-affected *Dsk7/+* mice having an ~0.3 mmol/L decrease in plasma calcium and ~65% reduction in PTH concentrations compared to +/+ mice, whereas homozygous-affected *Dsk7/Dsk7* mice have significantly more pronounced hypocalcemia (plasma calcium ~0.5 mmol/L lower than +/+ mice) and a greater (~85%) reduction in PTH concentrations (Figure 1, Table 1). The more severe hypocalcemia of homozygous-affected mice may potentially have affected their viability, thereby providing an explanation for the observed reduced numbers of mice with this genotype. The degree of hypocalcemia of affected *Dsk7* mice is similar to that of ADH2 patients, who have been reported to have serum calcium values ranging between 0.1-0.6 mmol/L below that of unaffected family members (7, 8, 27). Moreover, *Dsk7* mice generally had detectable circulating PTH concentrations and also a normal fractional excretion of calcium, which is in keeping with the majority of ADH2 patients (2, 7, 8). The markedly reduced circulating PTH of *Dsk7/Dsk7* mice was not significantly associated with decreases in plasma 1,25-dihydroxyvitamin D concentrations (Table 1), and such effects of PTH may have been counteracted by the low plasma FGF-23 concentrations, which would be expected to increase 1,25-dihydroxyvitamin D (28). Serum FGF-23 concentrations have not been reported for ADH2 patients, and our finding of low FGF-23 values in *Dsk7/Dsk7* mice was most likely a consequence of the hypocalcemia, which has been previously shown to reduce circulating FGF-23 concentrations in parathyroidectomized rats and in rats with hypocalcemia due to dietary calcium restriction (29). However, the mechanism by which hypocalcemia lowers FGF-23 remains to be established (29). The bone phenotype of ADH2 has been evaluated in a single kindred by plain radiography and no abnormalities were identified (19). Our

skeletal assessment of *Dsk7* mice also did not reveal any major alterations in BMD, trabecular volume or structure, which indicates that gain-of function $G\alpha_{11}$ mutations may not lead to alterations in bone metabolism.

In addition to *Dsk7* mice having similar calcitropic features to ADH2 patients, *Dsk7* mice may also share some non-calcitropic phenotypes with affected patients. Indeed, short stature has been reported in two ADH2 kindreds (7, 19), and in keeping with this, *Dsk7/Dsk7* mice have been previously noted to have significantly reduced body length and weight compared to +/+ mice (20). However, a key species-specific difference is that *Dsk7/+* and *Dsk7/Dsk7* mice have increased skin pigmentation, due to an expansion of the melanocyte population within the dermis (30), and such alterations in skin colour have not been reported for ADH2 patients to date. The studies of *Dsk7* mice and ADH2 patients have also revealed differences to the phenotype of ADH1, which is caused by gain-of-function *CASR* mutations (1, 9). In particular, ADH1 patients and knock-in mice harboring ADH1-causing *Casr* mutations, have been demonstrated to have a relative or absolute hypercalciuria, and high bone mass (1, 12), in addition to hypocalcemia and low circulating PTH concentrations. These alterations in parathyroid, renal and bone metabolism observed in ADH1 are in keeping with the known expression and function of the CaSR in these tissues (31-33). In contrast, our finding that *Dsk7* mice have hypocalcemia and low PTH values in the absence of renal or bone abnormalities, suggests that germline $G\alpha_{11}$ mutations may influence CaSR signaling responses in the parathyroid gland without perturbing the function of this GPCR in other calcitropic tissues (Figure 1, Table 1). In support of this, studies of mice with a parathyroid-specific ablation of the $G_{q/11}$ proteins (34), have demonstrated a critical role for these proteins in PTH secretion, whereas it remains to be established if these G-proteins act as a signaling partner for the CaSR in the kidneys and bone. Moreover, the lack of a renal or bone phenotype in *Dsk7* mice may also have been caused by alterations in the relative expression of $G\alpha_{11}$ and $G\alpha_q$. Thus, if $G\alpha_q$ expression predominates in kidney and bone, then a gain-of-function of $G\alpha_{11}$ may have been insufficient to alter CaSR signaling responses in these tissues. An additional difference in the phenotypes associated with gain-of-function mutations of the CaSR and $G\alpha_{11}$ proteins, respectively, is that *Nuf* mice, which have hypocalcemia in association with a germline *Casr* mutation, Leu723Gln, developed cataracts by 4-6 weeks of age (18), whereas *Dsk7* mice do not

have lens abnormalities. The CaSR has been reported to be expressed and functionally linked to Ca^{2+}-activated K^+ channels in lens epithelial cells (35), however its role in cataract formation has not been determined. The absence of lens opacifications in *Dsk7* mice indicates that alterations in CaSR-mediated $G\alpha_{11}$ signaling may not be involved in the development of this eye disorder.

Our findings help to elucidate some of the mechanisms whereby the germline Ile62Val $G\alpha_{11}$ mutation, which involves the substitution of amino acid residues with similar hydrophobic properties, cause a gain-of-function and enhance the sensitivity of CaSR expressing cells to Ca^{2+}_o. The WT $G\alpha_{11}$ Ile62 residue appears to be absolutely conserved amongst multicellular organisms, and is located within the Gα-subunit α1 helix at the interdomain interface, which contains a hydrophobic cluster of residues involved in guanine nucleotide binding (Figure 2) (23). Upon binding of G-protein to GPCR, the α1 helix has been shown to undergo conformational changes that destabilize the interdomain interface, thereby leading to the exchange of GDP for GTP (23), which triggers G-protein activation. It is likely that the Ile62Val mutation leads to a gain-of-function by decreasing the stability of the α1 helix, and this possibility is supported by reported mutagenesis studies involving the related $G\alpha_i$ protein, which have shown substitution of the homologous $G\alpha_i$ Ile residue with alanine to destabilize the GDP-bound form of the Gα-subunit (23). The $G\alpha_{11}$ interdomain interface and hydrophobic residue cluster represent a hotspot for gain-of-function mutations, with 5 out of 6 of the reported ADH2-causing mutations situated within this region (2, 7, 8, 10), consistent with our proposal that these mutations likely alter the conformation of the guanine nucleotide-binding pocket, thereby promoting GDP-GTP exchange and G-protein activation.

Although the Val62 $G\alpha_{11}$ mutant protein enhanced the Ca^{2+}_i responses of CaSR-expressing cells, consistent with a gain-of-function, it also significantly reduced the Hill coefficient, which was not rectifiable with calcilytic treatment (Figure 3). The Hill coefficient is commonly used to represent cooperative receptor-ligand interactions (36), but may also indicate the degree of interaction between a GPCR and its downstream partner signaling protein (25). Our finding of a reduced Hill coefficient suggests that the Ile62Val mutation may have altered coupling of the mutant $G\alpha_{11}$ protein with the CaSR. In support of this, ADH1-causing mutations located within the CaSR transmembrane domain,

which is predicted to be the site of G-protein binding, have also been reported to lower the Hill coefficient, whilst leading to a gain-of-function (37).

The most severe clinical manifestation of *GNA11* mutations is uveal melanoma, which is a malignant tumor arising from the melanocytes of the choroid plexus, ciliary body and iris, and caused by somatic mutations of the Arg183 and Qln209 $G\alpha_{11}$ residues that lead to constitutive upregulation of MAPK signaling (24). As the Ile62Val *Gna11* mutation is associated with increased proliferation of melanocyte precursors in *Dsk7* mice (20), we assessed the oncogenic potential of this mutation *in vitro*, and demonstrated that it increased MAPK responses only in the presence of Ca^{2+}_{o} stimulation (Figure 4). Thus, the Ile62Val $G\alpha_{11}$ mutant does not harbor constitutive activity, and these findings are consistent with previously reported ADH2 mutations, which also lead to a non-constitutive gain-of-function (7, 11), and are supported by studies of double mouse mutants, which have shown that the Ile62Val *Gna11* mutation does not cause increased skin pigmentation in the absence of an upstream functional receptor (20).

ADH2 is frequently associated with hypocalcemic symptoms such as paraesthesia, muscle cramps, carpo-pedal spasm and seizures (2, 7, 8, 10). However, treatment of symptomatic patients with calcium and active vitamin D preparations has resulted in adverse effects such as hypercalciuria, nephrocalcinosis and nephrolithiasis (7, 10). Although calcilytic compounds represented targeted therapies for patients with CaSR mutations causing symptomatic forms of ADH1 (12, 13), it was unclear if these CaSR allosteric modulators may rectify abnormalities of the downstream $G\alpha_{11}$ protein, and thus have potential benefit for ADH2 patients. Recent *in vitro* studies have revealed that low doses (10-30 nM concentrations) of the NPS-2143 calcilytic compound can successfully correct the gain-of-function associated with ADH2-causing $G\alpha_{11}$ mutations (11). Consistent with these findings, a similar dose of NPS-2143 also normalised the Ca^{2+}_{i} and MAPK responses of the Ile62Val $G\alpha_{11}$ mutant (Figure 3). Moreover, we have shown that administration of a single NPS-2143 dose induced a rapid and marked rise in PTH concentrations in *Dsk7/+* and *Dsk7/Dsk7* mice, and rectified or improved their hypocalcemic phenotypes, respectively (Figure 5); these data suggest that *Dsk7/Dsk7* mice will likely require a higher dose of NPS-2143 to correct their hypocalcaemia. These results suggest that calcilytics such as NPS-2143 will likely be of benefit for ADH2 patients, who also harbor

heterozygous *GNA11* mutations (2, 7, 8, 10). Oral administration of NPS-2143 was well tolerated, and the acute rise in plasma calcium post-dose did not affect the health or condition of the mice, or influence biochemical parameters such as electrolytes or renal function. However, an increase in plasma phosphate was noted in WT mice following treatment with NPS-2143, and this finding has also been reported in *Nuf* mice, which became hyperphosphatemic and had increases in urea and creatinine following a single i.p. injection of NPS-2143 (13). However, the rise in phosphate observed in the present study was not associated with alterations in renal function, and the cause of the hyperphosphatemia remains to be elucidated. Longer-term studies involving repetitive dosing are required to confirm the efficacy and safety of calcilytics for improving circulating calcium concentrations in the setting of ADH2. Of note, blood samples obtained from mice under isoflurane terminal anesthesia (Table 1) showed significant elevations in plasma concentrations of phosphate and PTH compared to samples obtained using topical local anesthesia (Supplementary Figure 5). General anesthetics, which include inhalation agents such as isoflurane, have been reported in laboratory animal studies to significantly alter plasma concentrations of phosphate and PTH (38, 39). Our findings further highlight the effects of anesthetic agents on these commonly measured biochemical parameters.

In conclusion, we have established that *Dsk7* mice, which harbor a germline gain-of-function $G\alpha_{11}$ mutation, represent an *in vivo* model for the human disorder of ADH2. We have also utilized this model to demonstrate that calcilytic compounds have the potential to treat the hypocalcemia associated with this disorder.

Methods

Animals

Dsk7 mice were re-derived on a C3H strain background (C3H.C3HeB/FeJ-Gna11^{Mhdadsk7}/IegH) by *in vitro* fertilisation using sperm obtained from the European Mutant Mouse Archive (EMMA). All study mice were aged between 12-16 weeks and housed in a controlled environment at the Medical Research Council (MRC) Harwell Institute in accordance with UK Home Office and MRC welfare guidance. Mice had free access to water and were fed *ad libitum* on a commercial diet (RM3, Special Diet Services, UK) that contained 1.15% calcium, 0.58% phosphate and 4089 IU/kg of vitamin D.

Compounds

NPS-2143 hydrochloride (also known as 2-Chloro-6-[(2R)-3-[[1,1-dimethyl-2-(2-naphthalenyl)ethyl]amino]-2-hydroxypropoxy]-benzonitrile hydrochloride) was obtained from Sigma-Aldrich (catalog no. SML0362) and dissolved in a 20% aqueous solution of 2-hydroxypropyl-β-cyclodextrin (Sigma-Aldrich, catalog no. H107) prior to use in *in vitro* and *in vivo* studies.

DNA sequence analysis

Genomic DNA was extracted from auricular biopsies, as described (40), and gene-specific primers were used to perform PCR amplification and DNA sequence analysis of *Gna11* exon 2, as reported (2). The germline *Gna11* mutation was confirmed by Fok*I* restriction endonuclease analysis (New England Biolabs), as previously described (20).

Protein Sequence Alignment and Three-dimensional modeling

Protein sequences of $G\alpha_{11}$ were aligned using ClustalOmega (http://www.ebi.ac.uk/Tools/msa/clustalo/) (41). PyMOL Molecular Graphics System (Version 1.2r3pre, Schrödinger, LL Pymol) (16) was used to model the effects of the $G\alpha_{11}$ Ile62Val mutation. $G\alpha_{11}$ three-dimensional modeling was undertaken using the reported three-dimensional structure of $G\alpha_q$ in complex with the small molecule inhibitor YM-254890 (Protein Data Bank accession no.

3AH8) (22) and also using the reported structure of the $G\alpha_i$ protein (Protein Data Bank accession no. 1GDD) (23).

Cell culture and protein expression

Functional studies were undertaken using a human *GNA11* construct (2), as the human and mouse $G\alpha_{11}$ proteins share an overall amino acid identity of 98%, and are 100% identical in the region surrounding the mutated site. The Val62 mutation was introduced by site-directed mutagenesis (QuikChange Lightning, Agilent Technologies) into a pBI-CMV2-*GNA11* expression construct, as described (2). WT and mutant pBI-CMV2-*GNA11* constructs were transiently transfected into HEK293 cells that stably express the full-length human *CASR* cDNA (HEK-CaSR), as described (2, 42, 43). HEK293 cells were used because suitable parathyroid and renal tubular cells are not available, and HEK293 cells have been established as a model for the functional expression of $G\alpha_{11}$ proteins (2, 43, 44). HEK-CaSR cells were cultured in high-glucose DMEM (Invitrogen) supplemented with 10% fetal bovine serum and 1% geneticin at 37°C, 5% CO_2 (2). Successful transfection was confirmed by visualising GFP fluorescence using an Eclipse E400 fluorescence microscope with an epifluorescence filter, and images were captured using a DXM1200C digital camera and NIS Elements software (Nikon) (2, 44). The expression of $G\alpha_{11}$ and CaSR proteins was confirmed by Western blot analyses using $G\alpha_{11}$ (D-6, sc-390382, Santa Cruz Biotechnologies), anti-GFP (B-2, sc-9996, Santa Cruz Biotechnologies), anti-calnexin (AB2301, Millipore), anti-GAPDH (AM4300, Ambion) or anti-CaSR (5C10, ADD, ab19347, Abcam) antibodies. The Western blots were visualised using an Immuno-Star Western C kit (BioRad) on a BioRad Chemidoc XRS+ system (2, 42). Densitometric analysis was performed using Image J analysis software (Version 1.46; rsb.info.nih.gov/ij/) and statistical analysis performed using two-way ANOVA, as previously described (45).

Measurement of Ca^{2+}_i responses

The effect of the mutant $G\alpha_{11}$ protein on the Ca^{2+}_i responses of CaSR-expressing cells was assessed by a flow cytometry-based assay, as reported (2, 43, 44). Briefly, 48h after transfection, the cells were

harvested, washed in calcium- and magnesium-free HBSS (Invitrogen) and loaded with 1 μ g/ml indo-1-acetoxymethylester (Indo-1-AM) (Molecular Probes) for 1h at 37°C (2, 43, 44). After the removal of free dye, the cells were resuspended in calcium- and magnesium-free HBSS and maintained at 37°C. Transfected HEK-CaSR cells were incubated with either a 20% aqueous solution of 2-hydoxypropyl- β -cyclodextrin (vehicle), or negative allosteric modulator NPS-2143 at concentrations of 20 and 40nM for 1h, as previously described (11).

Transfected cells in suspension were then stimulated by sequentially adding calcium to increase the $[Ca^{2+}]_o$ in a stepwise manner from 0 to 15 mM, and then analysed on a MoFlo modular flow cytometer (Beckman Coulter) by simultaneous measurement of GFP expression (at 525nm), $Ca^{2+}{}_i$-bound Indo-1AM (at 410nm), and free Indo-1AM (at 485nm), using a JDSU Xcyte UV laser (Coherent Radiation), on each cell at each $[Ca^{2+}]_o$, as described (2, 42, 43). Cytomation Summit software was used to determine the peak mean fluorescence ratio of the transient response after each individual stimulus expressed as a normalized response (2, 42, 43). Concentration-response curves were generated using a 4-parameter non-linear regression curve-fit model (GraphPad Prism) to calculate the half-maximal (EC_{50}) and Hill coefficient values (1, 7, 19). The maximal signaling response was measured as a fold-change of the peak transient $Ca^{2+}{}_i$ response to the basal $Ca^{2+}{}_i$ response. The maximal signaling response of mutant-expressing cells was expressed as a percentage of the WT maximal signaling response.

Measurement of ERK1/2 phosphorylation

HEK-CaSR cells were seeded in 48-well plates and transfected with 200ng WT or mutant $G\alpha_{11}$ proteins 24h prior to conducting the assays. Transfected cells were incubated in serum-free media 12h prior to treatment of cells with 0-10mM $CaCl_2$. Cells were lysed in Surefire lysis buffer, and AlphaScreen Surefire ERK assays measuring phosphorylated and total proteins were performed as previously described (11). For studies with negative allosteric modulators, cells were incubated with either a 20% aqueous solution of 2-hydoxypropyl- β -cyclodextrin (vehicle), or NPS-2143 for 4h prior to being stimulated with 10 mM $CaCl_2$. The fluorescence signal in both assays was measured using

the PheraStar FS microplate reader (BMG Labtech) (11, 45).

Measurement of serum response element (SRE) luciferase reporter activity

HEK-CaSR cells were seeded in 48-well plates and transiently transfected with 100ng/ml $G\alpha_{11}$ WT or mutant proteins, 100ng pGL4-*SRE* luciferase reporter construct and 10ng/ml pRL control vector for 48h. Cells were incubated in serum-free media for 12h, followed by treatment of cells for 4h with 0-10mM $CaCl_2$. Cells were lysed and assays performed using Dual-Glo luciferase (Promega) on a Veritas Luminometer (Promega), as previously described (44, 45).

Plasma biochemistry and hormone analysis

Blood samples were collected from the lateral tail vein of study mice following application of topical local anesthesia, as reported (40) or collected from the retro-orbital vein under isoflurane terminal anesthesia. Lateral tail vein sampling provides small volumes of blood that are adequate for analysis of plasma calcium, albumin, phosphate, PTH, urea and creatinine. However, retro-orbital vein sampling under terminal general anaesthesia, is required to obtain larger blood volumes that permit analysis of a wider range of biochemical parameters. Plasma was separated by centrifugation at 5000g for 10 min at 8°C, and analyzed for sodium, potassium, total calcium, magnesium, phosphate, urea, creatinine, albumin, and alkaline phosphatase on an Beckman Coulter AU680 analyzer, as described previously (13). Plasma calcium was adjusted for variations in albumin concentrations using the formula: (plasma calcium (mmol/L) – [(plasma albumin (g/L) – 30) x 0.02], as reported (40). Hormones were measured as follows: PTH using a two-site ELISA kit (Immunotopics); Intact FGF-23 using a two-site ELISA kit (Kainos Laboratoties, Tokyo, Japan); and 1,25-dihydroxyvitamin D measured by a two-step process involving purification by immunoextraction and quantification by enzyme immunoassay (Immunodiagnostic Systems, Boldon, UK), as described (46).

Metabolic cages and urine biochemistry analysis

Mice were individually housed in metabolic cages (Techniplast), and fed *ad libitum* on water and powdered chow. Mice were allowed to acclimatise to their environment over a 72h period, as

described (47), prior to collection of 24h urine samples. Urine was analyzed for sodium, potassium, creatinine, phosphate and calcium on a Beckman Coulter AU680 analyzer, as reported (18). The fractional excretion of sodium, potassium, and calcium were calculated using the formula $U_x/P_x*P_{Cr}/U_{Cr}$, where U_x is the urinary concentration of the filtered substance (substance *x*) in mmol/L, P_x is the plasma concentration of substance *x* in mmol/L, U_{Cr} is the urinary concentration of creatinine in mmol/L, and P_{Cr} is the plasma concentration of creatinine in mmol/L (13). The ratio of tubular maximum reabsorption of phosphate to GFR (TmP/GFR) was calculated using the following formula: $P_{Pi}*(1-(U_{Pi}/P_{Pi}*P_{Cr}/U_{Cr}))$, where P_{Pi} is the plasma concentration of phosphate and U_{Pi} is the urine concentration of phosphate.

Skeletal imaging

Bone mineral density was assessed by whole body DXA scanning, which was performed on mice anesthetized by inhaled isoflurane, and using a Lunar Piximus densitometer (GE Medical Systems), as reported (46). DXA images were analysed using Piximus software, as reported (46). Trabecular bone volume and structure were assessed by micro-CT analysis of the proximal tibia using a Skyscan 1174 scanner (SkyScan, Belgium), with X-ray settings 50kV, 800µA, 12.6 µm isometric voxel resolution, and 0.7 degree rotation step. The tibial trabecular region, located 1.5 mm distally from the growth plate, was selected for analysis, and a volume of interest was delineated by drawing within the cortex of the trabecular region. A threshold of 80-255 density units was selected to distinguish mineralized trabecular tissue from surrounding soft tissue of the marrow cavity. Cross-sectional images were obtained and 3-D reconstruction undertaken using Skyscan CT Analyzer software (version 1.9.3.0).

In vivo administration of NPS-2143

NPS-2143 was administered as a single 100 µmol/kg (~45 mg/kg) dose by oral gavage, or as a single 30 mg/kg dose by i.p. injection, as described (13), and plasma samples collected by tail vein bleed at either 0, 1, 2, 6 or 24h post-dose.

Statistical analysis

All *in vitro* studies involved between 2-12 separate transfection experiments and between 4-8 technical assays. For the *in vitro* measurement of Ca^{2+}_i EC_{50} responses, statistical comparisons were undertaken using the *F*-test (1, 7, 19), whereas, Ca^{2+}_i maximal signaling responses and Hill coefficients were analysed using the Mann-Whitney *U* test. Measurements of ERK phosphorylation and SRE gene luciferase reporter activity were analyzed using the Mann-Whitney *U* test or by 2-way ANOVA with Tukey's multiple-comparisons test. For the *in vivo* studies, a Kruskal-Wallis test was undertaken for multiple comparisons, and any significant differences identified were further assessed using the Dunn's test for non-parametric pairwise multiple comparisons. All analyses were undertaken using GraphPad Prism (GraphPad), and a value of $p<0.05$ was considered significant for all analyses.

Study approval

Animal studies were approved by the MRC Harwell Institute Ethical Review Committee and were licensed under the Animal (Scientific Procedures) Act 1986, issued by the UK Government Home Office Department (PPL30/3271).

Author Contributions

Designing research studies (C.M.G., F.M.H., S.A.H., M.A.N., T.L.V., R.D.C., R.V.T.), conducting experiments (C.M.G., S.A.H., V.N.B., S.E.P., A.R., A.J.F., N.R., M.S., A.P., T.A.H., S.W.), acquiring and analysing data (C.M.G., F.M.H., S.A.H., V.N.B., S.E.P.), wrote the manuscript (C.M.G., F.M.H., S.A.H., R.V.T.).

Acknowledgements

This work was supported by the United Kingdom Medical Research Council (MRC) programme grants - G9825289 and G1000467 (to M.A.N., F.M.H., C.M.G. and R.V.T), and National Institute for Health Research (NIHR) Oxford Biomedical Research Centre Programme (to M.A.N. and R.V.T.); European Commission Seventh Framework Programme (FP7-264663) (to V.N.B.); S.A.H. was a

Wellcome Trust Clinical Training Fellow; and R.V.T. is a Wellcome Trust Investigator and NIHR Senior Investigator.

References

1. Pearce SH, Williamson C, Kifor O, Bai M, Coulthard MG, Davies M, Lewis-Barned N, McCredie D, Powell H, Kendall-Taylor P, et al. A familial syndrome of hypocalcemia with hypercalciuria due to mutations in the calcium-sensing receptor. *N Engl J Med.* 1996;335(15):1115-22.
2. Nesbit MA, Hannan FM, Howles SA, Babinsky VN, Head RA, Cranston T, Rust N, Hobbs MR, Heath H, 3rd, and Thakker RV. Mutations affecting G-protein subunit alpha11 in hypercalcemia and hypocalcemia. *N Engl J Med.* 2013;368(26):2476-86.
3. Hofer AM, and Brown EM. Extracellular calcium sensing and signalling. *Nat Rev Mol Cell Biol.* 2003;4(7):530-8.
4. Raue F, Pichl J, Dorr HG, Schnabel D, Heidemann P, Hammersen G, Jaursch-Hancke C, Santen R, Schofl C, Wabitsch M, et al. Activating mutations in the calcium-sensing receptor: genetic and clinical spectrum in 25 patients with autosomal dominant hypocalcaemia - a German survey. *Clin Endocrinol (Oxf).* 2011;75(6):760-5.
5. Vargas-Poussou R, Huang C, Hulin P, Houillier P, Jeunemaitre X, Paillard M, Planelles G, Dechaux M, Miller RT, and Antignac C. Functional characterization of a calcium-sensing receptor mutation in severe autosomal dominant hypocalcemia with a Bartter-like syndrome. *J Am Soc Nephrol.* 2002;13(9):2259-66.
6. Watanabe S, Fukumoto S, Chang H, Takeuchi Y, Hasegawa Y, Okazaki R, Chikatsu N, and Fujita T. Association between activating mutations of calcium-sensing receptor and Bartter's syndrome. *Lancet.* 2002;360(9334):692-4.
7. Li D, Opas EE, Tuluc F, Metzger DL, Hou C, Hakonarson H, and Levine MA. Autosomal dominant hypoparathyroidism caused by germline mutation in GNA11: phenotypic and molecular characterization. *J Clin Endocrinol Metab.* 2014;99(9):E1774-83.
8. Mannstadt M, Harris M, Bravenboer B, Chitturi S, Dreijerink KM, Lambright DG, Lim ET, Daly MJ, Gabriel S, and Juppner H. Germline mutations affecting Galpha11 in hypoparathyroidism. *N Engl J Med.* 2013;368(26):2532-4.
9. Hannan FM, Nesbit MA, Zhang C, Cranston T, Curley AJ, Harding B, Fratter C, Rust N, Christie PT, Turner JJ, et al. Identification of 70 calcium-sensing receptor mutations in hyper- and hypo-calcaemic patients: evidence for clustering of extracellular domain mutations at calcium-binding sites. *Hum Mol Genet.* 2012;21(12):2768-78.
10. Piret SE, Gorvin CM, Pagnamenta AT, Howles SA, Cranston T, Rust N, Nesbit MA, Glaser B, Taylor JC, Buchs AE, et al. Identification of a G-Protein Subunit-alpha11 Gain-of-Function Mutation, Val340Met, in a Family with Autosomal Dominant Hypocalcemia Type 2 (ADH2). *J Bone Miner Res.* 2016;31(1207-14.
11. Babinsky VN, Hannan FM, Gorvin CM, Howles SA, Nesbit MA, Rust N, Hanyaloglu AC, Hu J, Spiegel AM, and Thakker RV. Allosteric Modulation of the Calcium-Sensing Receptor Rectifies Signaling Abnormalities Associated with G-protein alpha-11 Mutations causing Hypercalcemic and Hypocalcemic Disorders. *J Biol Chem.* 2016;291(10876-85.
12. Dong B, Endo I, Ohnishi Y, Kondo T, Hasegawa T, Amizuka N, Kiyonari H, Shioi G, Abe M, Fukumoto S, et al. Calcilytic Ameliorates Abnormalities of Mutant Calcium-Sensing Receptor (CaSR) Knock-in Mice Mimicking Autosomal Dominant Hypocalcemia (ADH). *J Bone Miner Res.* 2015;30(1980-93.
13. Hannan FM, Walls GV, Babinsky VN, Nesbit MA, Kallay E, Hough TA, Fraser WD, Cox RD, Hu J, Spiegel AM, et al. The Calcilytic Agent NPS 2143 Rectifies Hypocalcemia in a Mouse Model With an Activating Calcium-Sensing Receptor (CaSR) Mutation: Relevance to Autosomal Dominant Hypocalcemia Type 1 (ADH1). *Endocrinology.* 2015;156(9):3114-21.
14. Gowen M, Stroup GB, Dodds RA, James IE, Votta BJ, Smith BR, Bhatnagar PK, Lago AM, Callahan JF, DelMar EG, et al. Antagonizing the parathyroid calcium receptor stimulates parathyroid hormone secretion and bone formation in osteopenic rats. *J Clin Invest.* 2000;105(11):1595-604.
15. Nemeth EF, Delmar EG, Heaton WL, Miller MA, Lambert LD, Conklin RL, Gowen M, Gleason JG, Bhatnagar PK, and Fox J. Calcilytic compounds: potent and selective Ca2+

receptor antagonists that stimulate secretion of parathyroid hormone. *J Pharmacol Exp Ther.* 2001;299(1):323-31.
16. Kumar S, Matheny CJ, Hoffman SJ, Marquis RW, Schultz M, Liang X, Vasko JA, Stroup GB, Vaden VR, Haley H, et al. An orally active calcium-sensing receptor antagonist that transiently increases plasma concentrations of PTH and stimulates bone formation. *Bone.* 2010;46(2):534-42.
17. Nemeth EF, and Shoback D. Calcimimetic and calcilytic drugs for treating bone and mineral-related disorders. *Best Prac Res Clin Endocrinol Metab.* 2013;27(3):373-84.
18. Hough TA, Bogani D, Cheeseman MT, Favor J, Nesbit MA, Thakker RV, and Lyon MF. Activating calcium-sensing receptor mutation in the mouse is associated with cataracts and ectopic calcification. *Proc Natl Acad Sci U S A.* 2004;101(37):13566-71.
19. Tenhola S, Voutilainen R, Reyes M, Toiviainen-Salo S, Juppner H, and Makitie O. Impaired growth and intracranial calcifications in autosomal dominant hypocalcemia caused by a GNA11 mutation. *Eur J Endocrinol.* 2016;175(3):211-8.
20. Van Raamsdonk CD, Fitch KR, Fuchs H, de Angelis MH, and Barsh GS. Effects of G-protein mutations on skin color. *Nat Genet.* 2004;36(9):961-8.
21. Shoback DM, Bilezikian JP, Costa AG, Dempster D, Dralle H, Khan AA, Peacock M, Raffaelli M, Silva BC, Thakker RV, et al. Presentation of Hypoparathyroidism: Etiologies and Clinical Features. *J Clin Endocrinol Metab.* 2016;101(6):2300-12.
22. Nishimura A, Kitano K, Takasaki J, Taniguchi M, Mizuno N, Tago K, Hakoshima T, and Itoh H. Structural basis for the specific inhibition of heterotrimeric Gq protein by a small molecule. *Proc Natl Acad Sci U S A.* 2010;107(31):13666-71.
23. Sun D, Flock T, Deupi X, Maeda S, Matkovic M, Mendieta S, Mayer D, Dawson RJ, Schertler GF, Babu MM, et al. Probing Galphai1 protein activation at single-amino acid resolution. *Nat Struct Mol Biol.* 2015;22(9):686-94.
24. Van Raamsdonk CD, Griewank KG, Crosby MB, Garrido MC, Vemula S, Wiesner T, Obenauf AC, Wackernagel W, Green G, Bouvier N, et al. Mutations in GNA11 in uveal melanoma. *N Engl J Med.* 2010;363(23):2191-9.
25. Howles SA, Hannan FM, Babinsky VN, Rogers A, Gorvin CM, Rust N, Nesbit MA, Thakker RV, Richardson T, and McKenna MJ. Cinacalcet for Symptomatic Hypercalcemia Caused by AP2S1 Mutations. *N Engl J Med.* 2016;374(14):1396-8.
26. Loupy A, Ramakrishnan SK, Wootla B, Chambrey R, de la Faille R, Bourgeois S, Bruneval P, Mandet C, Christensen EI, Faure H, et al. PTH-independent regulation of blood calcium concentration by the calcium-sensing receptor. *J Clin Invest.* 2012;122(9):3355-67.
27. Hunter AG, Heick H, Poznanski WJ, and McLaine PN. Autosomal dominant hypoparathyroidism: a proband with concurrent nephrogenic diabetes insipidus. *J Med Genet.* 1981;18(6):431-5.
28. Quarles LD. Role of FGF23 in vitamin D and phosphate metabolism: implications in chronic kidney disease. *Exp Cell Res.* 2012;318(9):1040-8.
29. Rodriguez-Ortiz ME, Lopez I, Munoz-Castaneda JR, Martinez-Moreno JM, Ramirez AP, Pineda C, Canalejo A, Jaeger P, Aguilera-Tejero E, Rodriguez M, et al. Calcium deficiency reduces circulating levels of FGF23. *J Am Soc Nephrol.* 2012;23(7):1190-7.
30. Van Raamsdonk CD, Barsh GS, Wakamatsu K, and Ito S. Independent regulation of hair and skin color by two G protein-coupled pathways. *Pigment Cell Melanoma Res.* 2009;22(6):819-26.
31. Chang W, Tu C, Chen TH, Bikle D, and Shoback D. The extracellular calcium-sensing receptor (CaSR) is a critical modulator of skeletal development. *Sci Signal.* 2008;1(35):ra1.
32. Cheng Z, Liang N, Chen TH, Li A, Santa Maria C, You M, Ho H, Song F, Bikle D, Tu C, et al. Sex and age modify biochemical and skeletal manifestations of chronic hyperparathyroidism by altering target organ responses to Ca2+ and parathyroid hormone in mice. *J Bone Miner Res.* 2013;28(5):1087-100.
33. Toka HR, Al-Romaih K, Koshy JM, DiBartolo S, 3rd, Kos CH, Quinn SJ, Curhan GC, Mount DB, Brown EM, and Pollak MR. Deficiency of the calcium-sensing receptor in the kidney causes parathyroid hormone-independent hypocalciuria. *J Am Soc Nephrol.* 2012;23(11):1879-90.

34. Wettschureck N, Lee E, Libutti SK, Offermanns S, Robey PG, and Spiegel AM. Parathyroid-specific double knockout of Gq and G11 alpha-subunits leads to a phenotype resembling germline knockout of the extracellular Ca2+ -sensing receptor. *Mol Endocrinol.* 2007;21(1):274-80.
35. Chattopadhyay N, Ye C, Singh DP, Kifor O, Vassilev PM, Shinohara T, Chylack LT, Jr., and Brown EM. Expression of extracellular calcium-sensing receptor by human lens epithelial cells. *Biochem Biophys Res Commun.* 1997;233(3):801-5.
36. Huang Y, Zhou Y, Castiblanco A, Yang W, Brown EM, and Yang JJ. Multiple Ca(2+)-binding sites in the extracellular domain of the Ca(2+)-sensing receptor corresponding to cooperative Ca(2+) response. *Biochemistry.* 2009;48(2):388-98.
37. Leach K, Wen A, Davey AE, Sexton PM, Conigrave AD, and Christopoulos A. Identification of molecular phenotypes and biased signaling induced by naturally occurring mutations of the human calcium-sensing receptor. *Endocrinology.* 2012;153(9):4304-16.
38. Gil AG, Silvan G, Villa A, Millan P, Martinez-Fernandez L, and Illera JC. Serum biochemical response to inhalant anesthetics in New Zealand white rabbits. *J Am Assoc Lab Anim Sci.* 2010;49(1):52-6.
39. Schultz VL, Boass A, Garner SC, and Toverud SU. Several anesthetics, but not diethyl ether, cause marked elevation of serum parathyroid hormone concentration in rats. *J Bone Miner Res.* 1995;10(9):1298-302.
40. Bentley L, Esapa CT, Nesbit MA, Head RA, Evans H, Lath D, Scudamore CL, Hough TA, Podrini C, Hannan FM, et al. An N-ethyl-N-nitrosourea induced corticotropin-releasing hormone promoter mutation provides a mouse model for endogenous glucocorticoid excess. *Endocrinology.* 2014;155(3):908-22.
41. Sievers F, Wilm A, Dineen D, Gibson TJ, Karplus K, Li W, Lopez R, McWilliam H, Remmert M, Soding J, et al. Fast, scalable generation of high-quality protein multiple sequence alignments using Clustal Omega. *Mol Syst Biol.* 2011;7(539.
42. Gorvin CM, Cranston T, Hannan FM, Rust N, Qureshi A, Nesbit MA, and Thakker RV. G-Protein Subunit-alpha11 Loss-of-Function Mutation, Thr54Met, Causing Familial Hypocalciuric Hypercalcemia Type 2 (FHH2). *J Bone Miner Res.* 2016;31(1200-6.
43. Nesbit MA, Hannan FM, Howles SA, Reed AA, Cranston T, Thakker CE, Gregory L, Rimmer AJ, Rust N, Graham U, et al. Mutations in AP2S1 cause familial hypocalciuric hypercalcemia type 3. *Nat Genet.* 2013;45(1):93-7.
44. Hannan FM, Howles SA, Rogers A, Cranston T, Gorvin CM, Babinsky VN, Reed AA, Thakker CE, Bockenhauer D, Brown RS, et al. Adaptor protein-2 sigma subunit mutations causing familial hypocalciuric hypercalcaemia type 3 (FHH3) demonstrate genotype-phenotype correlations, codon bias and dominant-negative effects. *Hum Mol Genet.* 2015;24(18):5079-92.
45. Newey PJ, Gorvin CM, Cleland SJ, Willberg CB, Bridge M, Azharuddin M, Drummond RS, van der Merwe PA, Klenerman P, Bountra C, et al. Mutant prolactin receptor and familial hyperprolactinemia. *N Engl J Med.* 2013;369(21):2012-20.
46. Esapa CT, Hannan FM, Babinsky VN, Potter P, Thomas GP, Croucher PI, Brown MA, Brown SD, Cox RD, and Thakker RV. N-ethyl-N-Nitrosourea (ENU) induced mutations within the klotho gene lead to ectopic calcification and reduced lifespan in mouse models. *PLoS One.* 2015;10(4):e0122650.
47. Stechman MJ, Ahmad BN, Loh NY, Reed AA, Stewart M, Wells S, Hough T, Bentley L, Cox RD, Brown SD, et al. Establishing normal plasma and 24-hour urinary biochemistry ranges in C3H, BALB/c and C57BL/6J mice following acclimatization in metabolic cages. *Lab Anim.* 2010;44(3):218-25.

Figure legends

Figure 1. Calcitropic phenotype of *Dsk7* mice. (A-B) plasma adjusted-calcium, (C-D) plasma phosphate, and (E-F) plasma PTH concentrations of male and female WT (+/+, circles), *Dsk7/+* (squares) and *Dsk7/Dsk7* (triangles) mice, respectively. Mean ± SEM values for the respective groups are indicated by the solid bars. *P < 0.05, **P < 0·01. ***P < 0.001. A Kruskal-Wallis test followed by Dunn's test for non-parametric pairwise multiple comparisons were used for analysis of A-F.

Figure 2. Structural characterization of the Ile62Val Gα_{11} mutation. (A) Genomic organization of *Gna11* showing location of the Ile62Val mutation. The Gα_{11} GTPase domain (encoded by exon 1, 5' portion of exon 2, 3' portion of exon 4 and exons 5 to 7) is connected to the helical domain (encoded by the 3' portion of exon 2, exon 3, and 5' portion of exon 4) by the linker 1 (L1) and 2 (L2) peptides. The Ile62Val mutation (red) lies within the α1-helix (green). The location of reported ADH2 mutations are indicated (black). (B) Multiple protein sequence alignment of residues comprising the α1 helix and L1 peptide of Gα_{11}-subunit orthologs (top) and Gα-subunit paralogs (bottom). Conserved residues are shown in gray. The WT (Ile) and Dsk7 mutant (m) (Val) residues are shown in red. (C) Homology model of the Gα_{11} protein. The Gα helical (blue) and GTPase (green) domains are connected by the L1 and L2 peptides (gray). GDP (black) is bound at the interdomain interface. Previously reported residues mutated in ADH2 are shown in yellow. The mutated Ile62 residue is shown in red. (D) Close-up view of the Ile62 residue which lies within a hydrophobic cluster of residues (blue spheres) on α1, α5 and β1 of the GTPase domain, and near to the interdomain interface (dotted line) and GDP binding site.

Figure 3. Intracellular calcium responses of the Val62 Gα_{11} mutant and effect of NPS-2143 treatment. (A) Fluorescence microscopy of HEK293 cells stably expressing CaSR (HEK-CaSR) and transiently transfected with WT Ile62 or mutant (m) Val62 pBI-CMV2-*GNA11* constructs. GFP expression in these cells indicates successful transfection and expression by these constructs. Bar indicates 10μm. (B) Western blot analysis of lysates from HEK-CaSR cells used for flow cytometry

experiments. Transient transfection with WT or mutant Val62 expression constructs resulted in overexpression of $G\alpha_{11}$ and GFP. Calnexin, a housekeeping protein, and untransfected cells (Supplementary Figure 2) were used as controls. (C) $Ca^{2+}{}_i$ response to changes in $[Ca^{2+}]_o$ of HEK-CaSR cells transfected with WT or Val62 $G\alpha_{11}$ mutant. The $Ca^{2+}{}_i$ responses to changes in $[Ca^{2+}]_o$ are expressed as a percentage of the maximum normalized responses and shown as the mean ± SEM of 5-8 assays from two independent transfections. The Val62 $G\alpha_{11}$ mutant led to a leftward shift in the concentration-response curve (red line). The addition of 20 nM NPS-2143 rectified the leftward shift of the Val62 $G\alpha_{11}$ mutant (red dashed line), whereas 40 nM NPS-2143 led to a rightward shift of the mutant concentration-response curve (pink dashed line) compared to WT (black line). (D-F) Histograms showing mean ± SEM EC_{50} values, % maximal signaling responses, and Hill coefficients, respectively, for cells expressing WT (open bar) or Val62 $G\alpha_{11}$ mutant (black bar) proteins, and for mutant-expressing cells treated with NPS-2143 (patterned bars). **P < 0.01, ***P <0.001. F-test for C-D. Mann-Whitney U test for E-F.

Figure 4. MAPK responses of the Val62 $G\alpha_{11}$ mutant and effect of NPS-2143 treatment. (A) Western blot analysis of lysates from HEK-CaSR cells used for phospho-ERK (pERK) experiments. (B) pERK fold-change responses to changes in $[Ca^{2+}]_o$ of cells transfected with WT (solid line) or Val62 $G\alpha_{11}$ mutant (dashed line). (C) Western blot analysis of lysates from cells used to assess effect of NPS-2143 (2143) on pERK responses (D) Effect of NPS-2143 on pERK responses of Val62 $G\alpha_{11}$ mutant. (E) Western blot analysis of lysates from HEK-CaSR cells used for serum response element reporter experiments. (F) SRE reporter fold-change responses to changes in $[Ca^{2+}]_o$ of cells transfected with WT (solid line) or Val62 $G\alpha_{11}$ mutant (dashed line). (G) Western blot analysis of lysates from cells used to assess effect of NPS-2143 on SRE reporter responses. (H) Effect of NPS-2143 on the SRE reporter responses of the Val62 $G\alpha_{11}$ mutant. The Val62 $G\alpha_{11}$ mutant led to significantly increased pERK and SRE fold-change responses following stimulation with $Ca^{2+}{}_o$. In the absence of $Ca^{2+}{}_o$, the pERK and SRE responses of the Val62 $G\alpha_{11}$ mutant were not significantly different from WT, thereby indicating the Ile62Val $G\alpha_{11}$ mutation to be non-constitutively activating. The addition of 20 nM NPS-2143 decreased the pERK and SRE responses of cells expressing the

Val62 $G\alpha_{11}$ mutant (patterned bars) compared to untreated cells (solid bars), so that these were not significantly different from WT (open bars). The fold-change responses are shown as the mean ± SEM of 4-8 independent transfections. *P < 0.05, **P < 0.01. Mann-Whitney U test for B, D, F and H.

Figure 5. Effect of NPS-2143 on plasma PTH, calcium and phosphate of *Dsk7* mice at 0, 1, 2, 6 and 24h post-dose. (A-C) plasma PTH, (D-F) plasma adjusted-calcium, and (G-I) plasma phosphate concentrations of WT (+/+), *Dsk7/+* and *Dsk7/Dsk7* mice, respectively. Mean values for the respective groups are indicated by solid bars. N=4-7 mice per study time-point. Squares, males; circles, females. *P < 0.05, **P < 0·01. A Kruskal-Wallis test followed by Dunn's test for non-parametric pairwise multiple comparisons were used for analysis of A-I.

Table 1. Age, weight and plasma biochemical profile of WT and *Dsk7* mice

	Male			**Female**		
	+/+	***Dsk7/+***	***Dsk7/Dsk7***	+/+	***Dsk7/+***	***Dsk7/Dsk7***
Age (weeks)	13.6±0.2 (n=27)	13.5±0.2 (n=29)	13.5±0.3 (n=17)	13.7±0.3 (n=24)	13.7±0.2 (n=31)	13.7±0.2 (n=20)
Weight (g)	32.2±0.4 (n=11)	33.9±0.6 (n=12)	28.9±0.9*** (n=10)	30.8±0.4 (n=11)	29.4±1.1 (n=12)	24.6±0.9* (n=7)
Plasma biochemistry						
Sodium (mmol/L)	151±0.4 (n=12)	151±0.9 (n=13)	150±0.2 (n=9)	148±1.1 (n=11)	146±1.3 (n=12)	150±1.2 (n=7)
Potassium (mmol/L)	5.5±0.1 (n=13)	5.2±0.1 (n=12)	5.0±0.1 (n=10)	4.5±0.2 (n=11)	4.9±0.3 (n=11)	4.5±0.2 (n=7)
Urea (mmol/L)	12.6±0.4 (n=12)	11.5±0.4 (n=13)	12.9±0.2 (n=9)	9.1±0.6 (n=11)	8.7±0.8 (n=12)	10.9±1.0 (n=7)
Creatinine (µmol/L)	11.9±0.5 (n=13)	12.1±0.8 (n=12)	12.8±0.5 (n=10)	11.6±0.6 (n=11)	11.8±0.5 (n=12)	12.9±1.3 (n=7)
Calcium (mmol/L)[A]	2.51±0.02 (n=25)	2.20±0.01*** (n=25)	1.98±0.05*** (n=15)	2.45+0.03 (n=22)	2.19±0.02*** (n=29)	1.90±0.03*** (n=17)
Magnesium(mmol/L)	0.86±0.02 (n=11)	0.82±0.02 (n=14)	0.87±0.02 (n=6)	0.87±0.02 (n=10)	0.83±0.01 (n=17)	0.78±0.02 (n=10)
Phosphate (mmol/L)	2.23±0.1 (n=20)	3.01±0.07** (n=22)	3.96±0.24*** (n=13)	2.43±0.07 (n=13)	2.89±0.1* (n=19)	3.19±0.19** (n=15)
ALP (U/L)	93.2±2.3 (n=12)	95.3±2.8 (n=13)	93.3±5.2 (n=10)	120±8.4 (n=11)	127±4.9 (n=12)	121±8.5 (n=7)
PTH (ng/L)	404±44 (n=12)	133±13** (n=12)	64±19*** (n=6)	283±41 (n=11)	158±21* (n=16)	50±9*** (n=12)
1,25D (pmol/L)	109±15 (n=14)	86±11 (n=13)	59±11 (n=5)	85±9 (n=13)	58±6 (n=16)	60±12 (n=12)
FGF-23 (ng/L)	270±45 (n=10)	174±23 (n=13)	120±29[$] (n=6)	200±39 (n=11)	110±14 (n=18)	74±13* (n=8)

[A]Plasma calcium concentrations were adjusted for the plasma albumin concentration. ALP, alkaline phosphatase activity; PTH, parathyroid hormone; 1,25D, 1,25 dihydroxyvitamin D; FGF-23, fibroblast growth factor-23. All values are expressed as mean ± SEM. [$]P = 0.05; *P < 0.05, **P < 0.01, ***P < 0.001 compared to respective WT (+/+) mice. A Kruskal-Wallis test followed by Dunn's test for non-parametric pairwise multiple comparisons were used for all analyses.

Table 2. Urine biochemical profile of WT and *Dsk7* mice

	Male			**Female**		
	+/+	***Dsk7/+***	***Dsk7/Dsk7***	+/+	***Dsk7/+***	***Dsk7/Dsk7***
24hr Ca	2.14±0.28 (n=13)	1.99±0.23 (n=13)	2.0±0.23 (n=10)	2.71±0.24 (n=11)	1.70±0.20* (n=12)	1.78±0.32 (n=7)
Ca/Cr	0.22±0.01 (n=12)	0.22±0.02 (n=13)	0.23±0.03 (n=10)	0.29±0.03 (n=11)	0.19±0.01* (n=12)	0.23±0.03 (n=7)
FECa	0.001±0.0001 (n=12)	0.001±0.0001 (n=12)	0.001±0.0002 (n=9)	0.001±0.0001 (n=11)	0.001±0.0003 (n=12)	0.002±0.0002 (n=7)
FENa	0.004±0.0002 (n=13)	0.004±0.0001 (n=12)	0.004±0.0002 (n=10)	0.003±0.0002 (n=11)	0.004±0.0002 (n=12)	0.004±0.0004 (n=7)
FEK	0.14±0.006 (n=13)	0.14±0.007 (n=12)	0.18±0.02 (n=10)	0.12±0.007 (n=11)	0.14±0.007 (n=11)	0.14±0.009 (n=7)
TmP/GFR	2.4±0.2 (n=13)	3.0±0.1* (n=13)	4.3±0.2*** (n=10)	2.4±0.1 (n=11)	3.1±0.1** (n=12)	3.7±0.2*** (n=7)

Parameters were measured using urine samples obtained over a 24-hour period. Urinary calcium excretion values are shown as µmol/24 hours. Calcium/creatinine ratios (Ca/Cr) are shown as mmol/mmol. FE, fractional excretion; TmP/GFR, ratio of tubular maximum reabsorption of phosphate (TmP) to GFR. All values are expressed as mean ± SEM. *P < 0.05, **P < 0.01, ***P < 0.001 compared to respective WT (+/+) mice. A Kruskal-Wallis test followed by Dunn's test for non-parametric pairwise multiple comparisons were used for all analyses.

Table 3. Bone parameters of WT and *Dsk7* mice

	Male			**Female**		
	+/+	***Dsk7/+***	***Dsk7/Dsk7***	+/+	***Dsk7/+***	***Dsk7/Dsk7***
Whole body DXA						
BMD (g/cm^2)	0.064±0.001 (n=6)	0.063±0.002 (n=6)	0.061±0.001 (n=4)	0.062±0.002 (n=10)	0.065±0.002 (n=10)	0.058±0.003 (n=5)
Proximal tibia micro-CT						
BV (mm^3)	0.78±0.04 (n=6)	0.71±0.04 (n=6)	0.65±0.03 (n=6)	1.10±0.08 (n=6)	1.10±0.08 (n=6)	1.10±0.06 (n=6)
BV/TV (%)	27±1.7 (n=6)	27±1.0 (n=6)	29±2.1 (n=6)	50±3.7 (n=6)	52±2.3 (n=6)	60±1.0 (n=6)
Tb. Th (mm)	0.10±0.001 (n=6)	0.98±0.002 (n=6)	0.10±0.003 (n=6)	0.14±0.005 (n=6)	0.15±0.005 (n=6)	0.16±0.006 (n=6)
Tb. N (mm^{-1})	2.7±0.1 (n=6)	2.7±0.1 (n=6)	2.8±0.1 (n=6)	3.5±0.1 (n=6)	3.5±0.1 (n=6)	3.6±0.1 (n=6)
SMI	1.9±0.2 (n=6)	1.7±0.1 (n=6)	1.8±0.1 (n=6)	0.7±0.2 (n=6)	0.5±0.2 (n=6)	-0.1±0.2 (n=6)

DXA, dual-energy X-ray absorptiometry; BMD, bone mineral density; BV, bone volume; BV/TV, cancellous bone volume fraction as a proportion of total possible organ ("tissue") volume; Tb. Th, trabecular thickness; Tb. N, trabecular number; SMI, structural model index. All values are expressed as mean ± SEM. A Kruskal-Wallis test followed by Dunn's test for non-parametric pairwise multiple comparisons were used for all analyses.

Figure 1

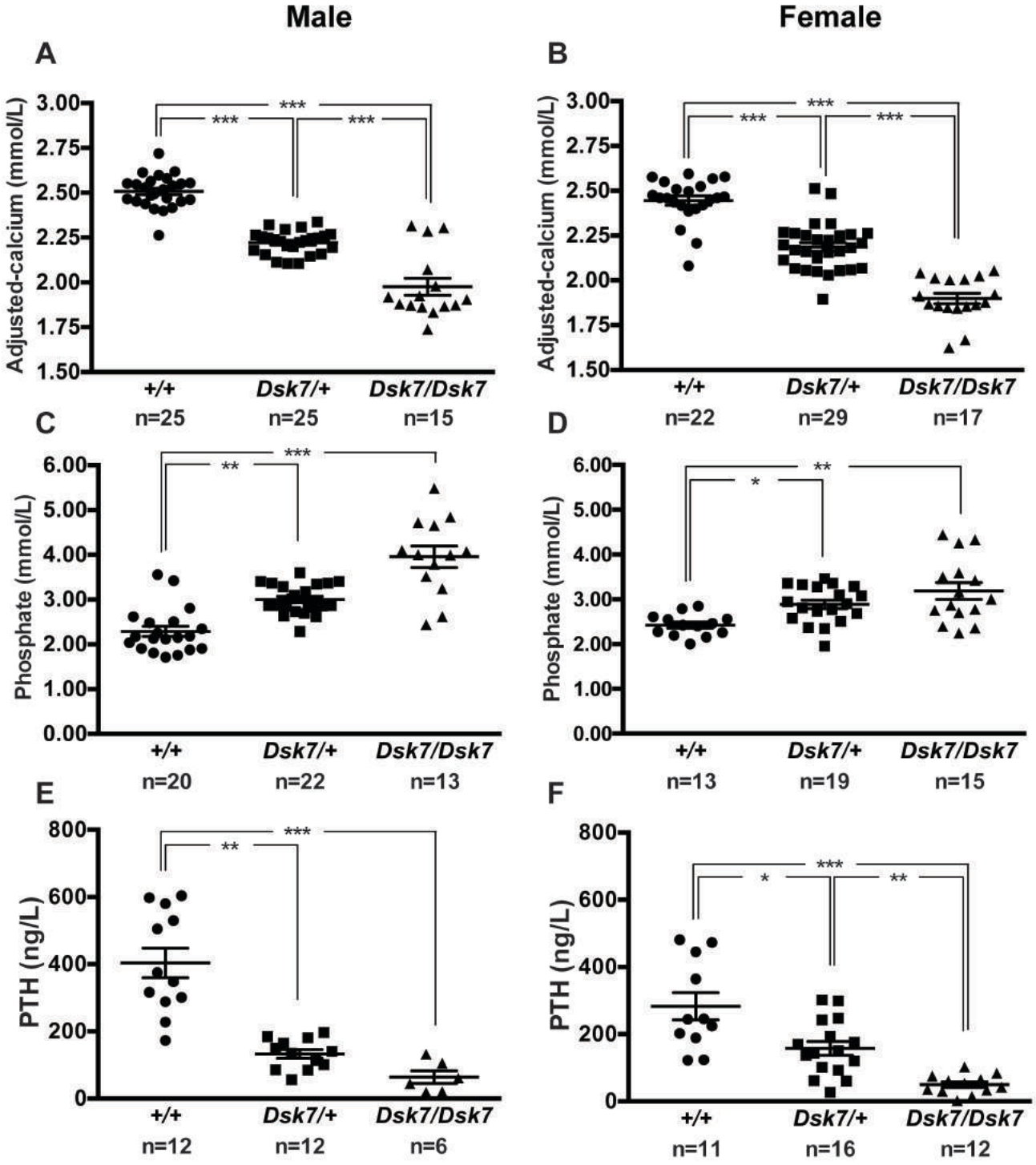
Male
Female
A
B
C
D
E
F
Adjusted-calcium (mmol/L)
Phosphate (mmol/L)
PTH (ng/L)
+/+
Dsk7/+
Dsk7/Dsk7
n=25
n=25
n=15
n=22
n=29
n=17
n=20
n=22
n=13
n=13
n=19
n=15
n=12
n=12
n=6
n=11
n=16
n=12

Figure 2

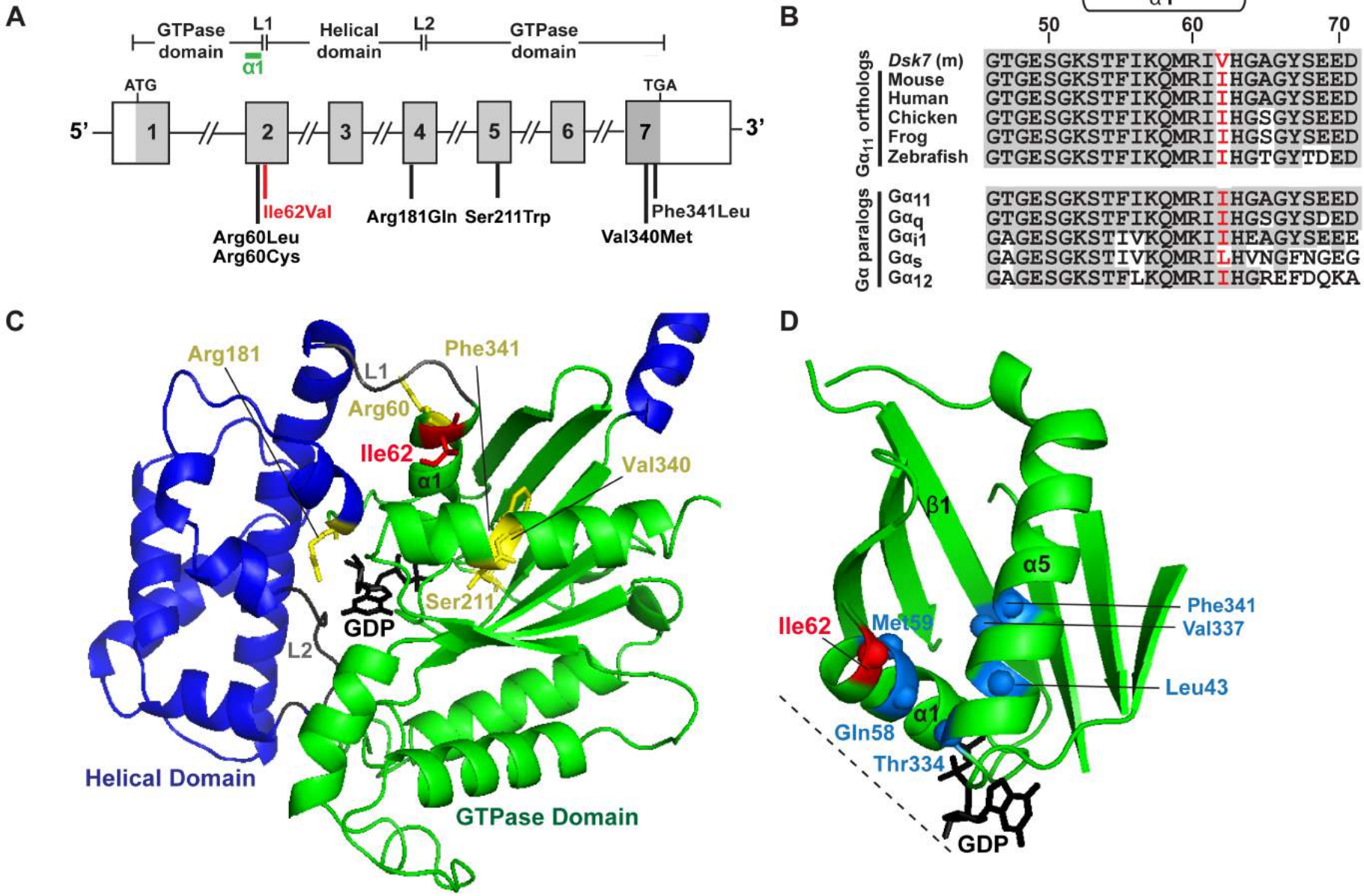
A
GTPase domain
L1
α1
Helical domain
L2
GTPase domain
ATG
TGA
5'
1
2
3
4
5
6
7
3'
Ile62Val
Arg60Leu
Arg60Cys
Arg181Gln
Ser211Trp
Phe341Leu
Val340Met
B
α1
L1
50
60
70
Gα11 orthologs
Dsk7 (m) GTGESGKSTFIKQMRIVHGAGYSEED
Mouse GTGESGKSTFIKQMRIIHGAGYSEED
Human GTGESGKSTFIKQMRIIHGAGYSEED
Chicken GTGESGKSTFIKQMRIIHGSGYSEED
Frog GTGESGKSTFIKQMRIIHGSGYSEED
Zebrafish GTGESGKSTFIKQMRIIHGTGYTDED
Gα paralogs
Gα11 GTGESGKSTFIKQMRIIHGAGYSEED
Gαq GTGESGKSTFIKQMRIIHGSGYSDED
Gαi1 GAGESGKSTIVKQMKIIHEAGYSEEE
Gαs GAGESGKSTIVKQMRILHVNGFNGEG
Gα12 GAGESGKSTFLKQMRIIHGREFDQKA
C
Arg181
L1
Phe341
Arg60
Ile62
α1
Val340
Ser211
GDP
L2
Helical Domain
GTPase Domain
D
β1
α5
Phe341
Val337
Ile62
Met59
Leu43
α1
Gln58
Thr334
GDP

Figure 3

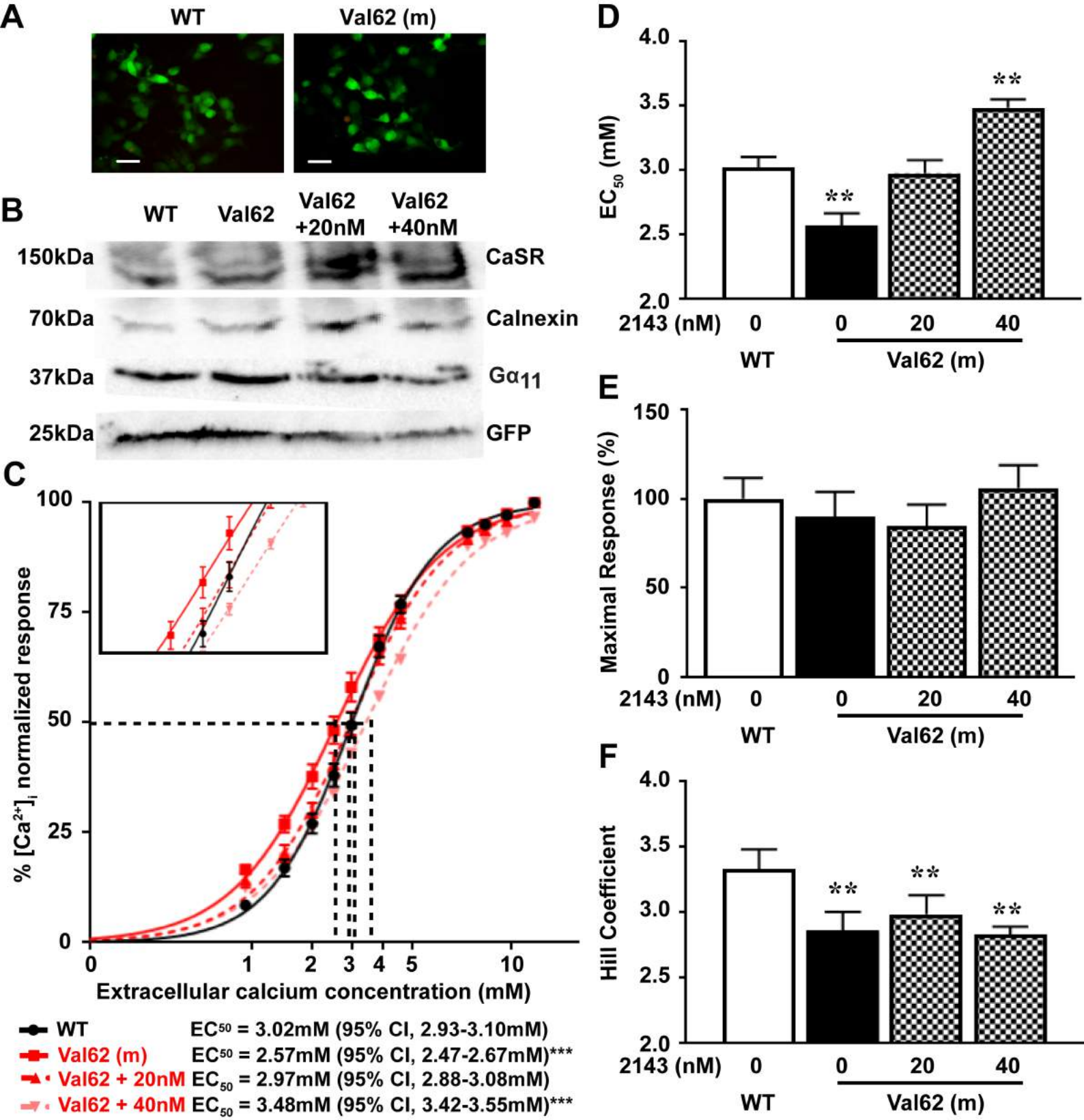
A
WT
Val62 (m)
B
WT
Val62
Val62 +20nM
Val62 +40nM
150kDa
CaSR
70kDa
Calnexin
37kDa
Gα11
25kDa
GFP
C
% [Ca2+]i normalized response
Extracellular calcium concentration (mM)
WT EC50 = 3.02mM (95% CI, 2.93-3.10mM)
Val62 (m) EC50 = 2.57mM (95% CI, 2.47-2.67mM)***
Val62 + 20nM EC50 = 2.97mM (95% CI, 2.88-3.08mM)
Val62 + 40nM EC50 = 3.48mM (95% CI, 3.42-3.55mM)***
D
EC50 (mM)
2143 (nM)
WT
Val62 (m)
E
Maximal Response (%)
F
Hill Coefficient

Figure 4

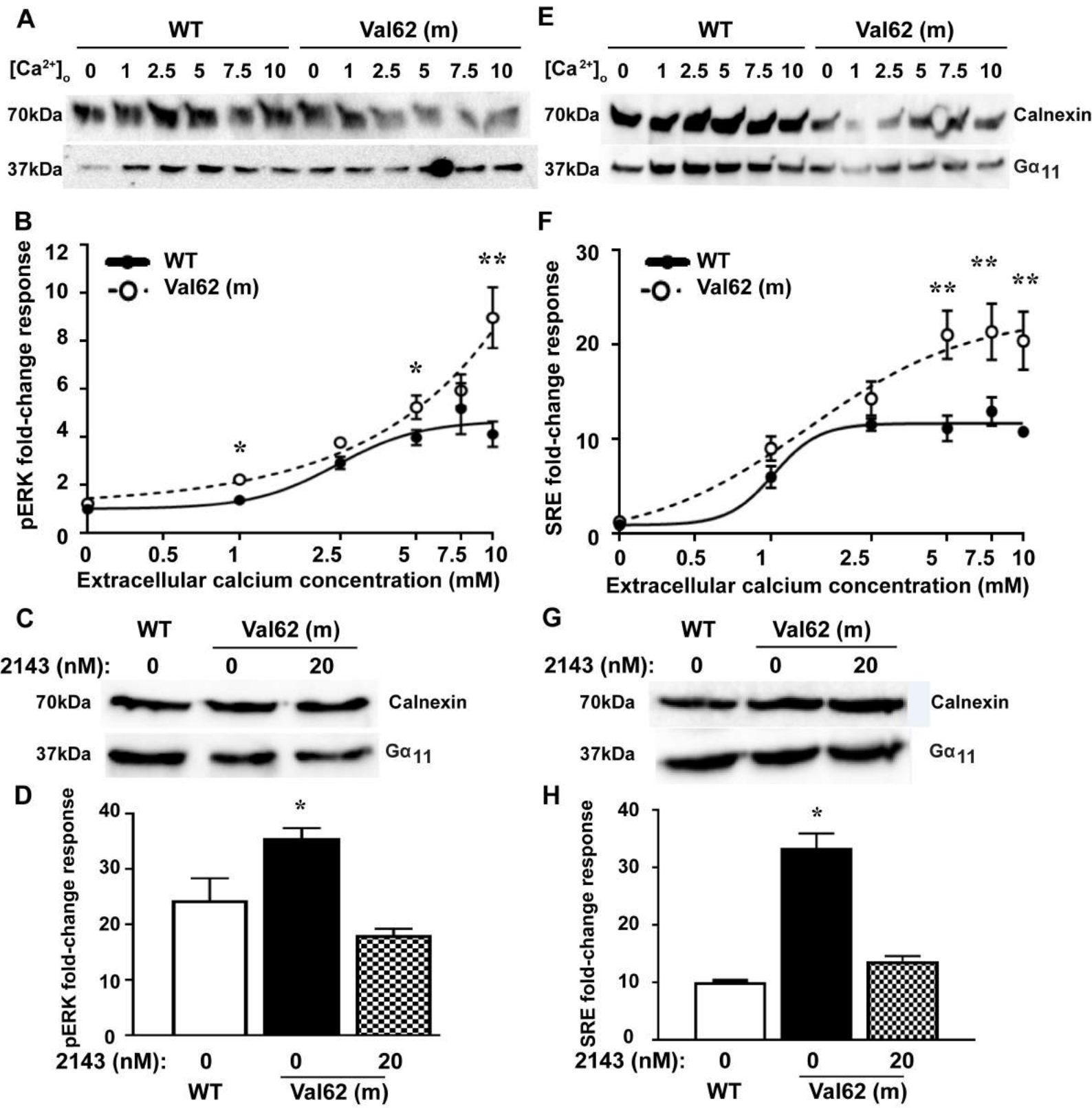
A
WT
Val62 (m)
[Ca2+]o 0 1 2.5 5 7.5 10 0 1 2.5 5 7.5 10
70kDa
37kDa
E
WT
Val62 (m)
[Ca2+]o 0 1 2.5 5 7.5 10 0 1 2.5 5 7.5 10
70kDa
Calnexin
37kDa
Gα11
B
pERK fold-change response
WT
Val62 (m)
Extracellular calcium concentration (mM)
F
SRE fold-change response
WT
Val62 (m)
Extracellular calcium concentration (mM)
C
WT
Val62 (m)
2143 (nM): 0 0 20
70kDa
Calnexin
37kDa
Gα11
G
WT
Val62 (m)
2143 (nM): 0 0 20
70kDa
Calnexin
37kDa
Gα11
D
pERK fold-change response
2143 (nM): 0 0 20
WT
Val62 (m)
H
SRE fold-change response
2143 (nM): 0 0 20
WT
Val62 (m)

Figure 5

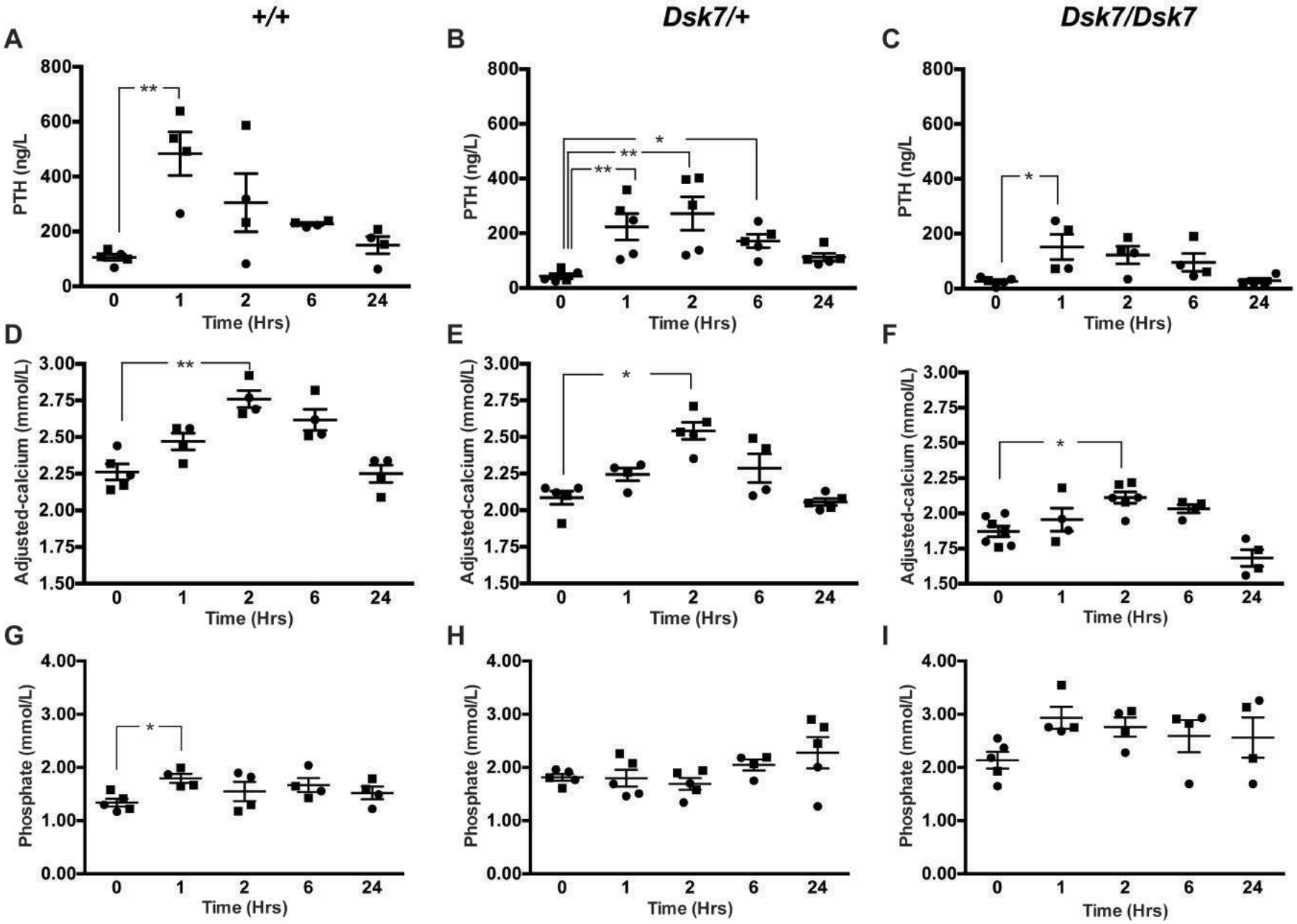
+/+
Dsk7/+
Dsk7/Dsk7
A
B
C
D
E
F
G
H
I
PTH (ng/L
Adjusted-calcium (mmol/L)
Phosphate (mmol/L)
Time (Hrs)
0
1
2
6
24
**
*

Supplementary Table 1. Proportion of offspring bred from crosses of *Dsk7/+* x *Dsk7/+* mice

Genotype	Expected number of offspring (n=584 born)	Observed number of offspring (n=482 weaned)
+/+	146 (25%)	128 (27%)
Dsk7/+	292 (50%)	272 (56%)
Dsk7/Dsk7	146 (25%)	82 (17%)

Chi-square analysis showed the observed proportion of offspring to be different from those expected ($x^2 = 10.20$, $df = 2$, $P < 0.01$), with significantly fewer *Dsk7/Dsk7* mice being bred.

Supplementary Figure 1

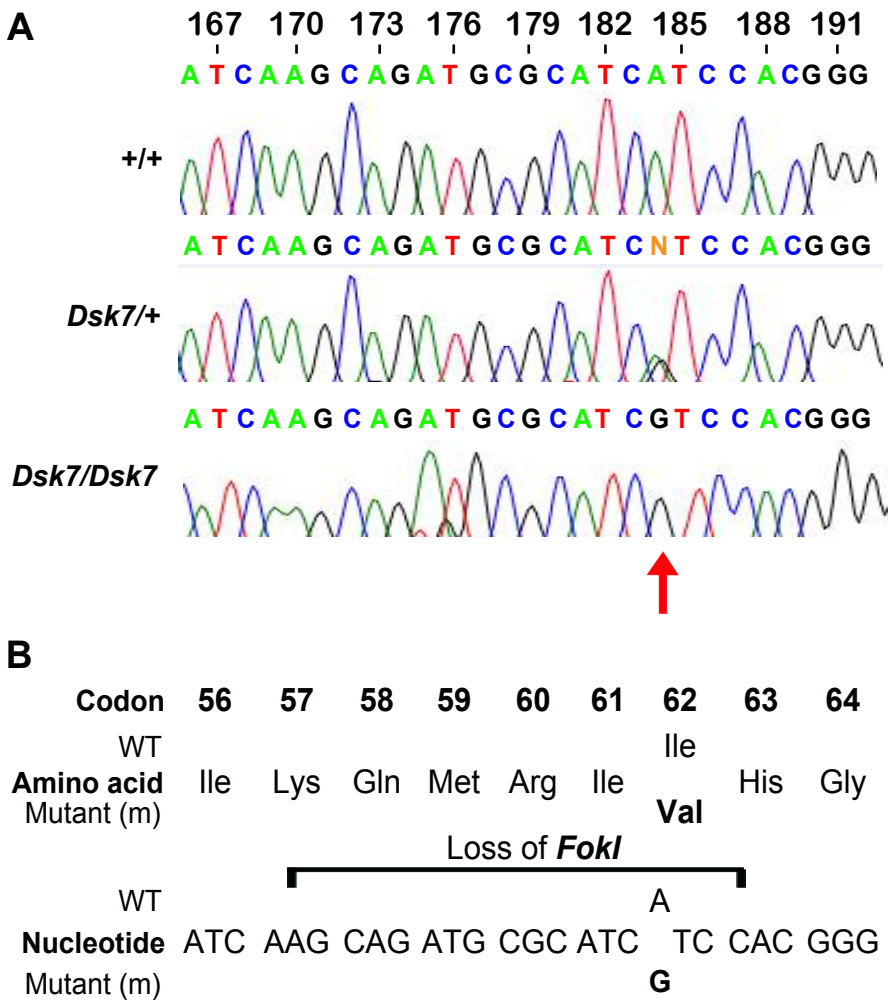

Supplementary Figure 1. DNA sequence and restriction endonuclease analysis of the Val62 Gα11 mutation. (**A**) DNA sequence analysis showed an A-to-G transition at c.184 (red arrow) within exon 2 of *Gna11*. (**B**) This sequence abnormality was predicted to lead to a missense substitution of Ile to Val at codon 62, resulting in the loss of a FokI restriction endonuclease (RE) site. (**C**) Restriction maps showing FokI digest would result in two products of 66bp and 160bp for the WT, and one 226bp product for the mutant (m). (**D**) RE digest of Gna11 exon 2 PCR products demonstrating the A-to-G transition in Dsk7/+ and Dsk7/Dsk7 mice. S = size marker.

Supplementary Figure 2

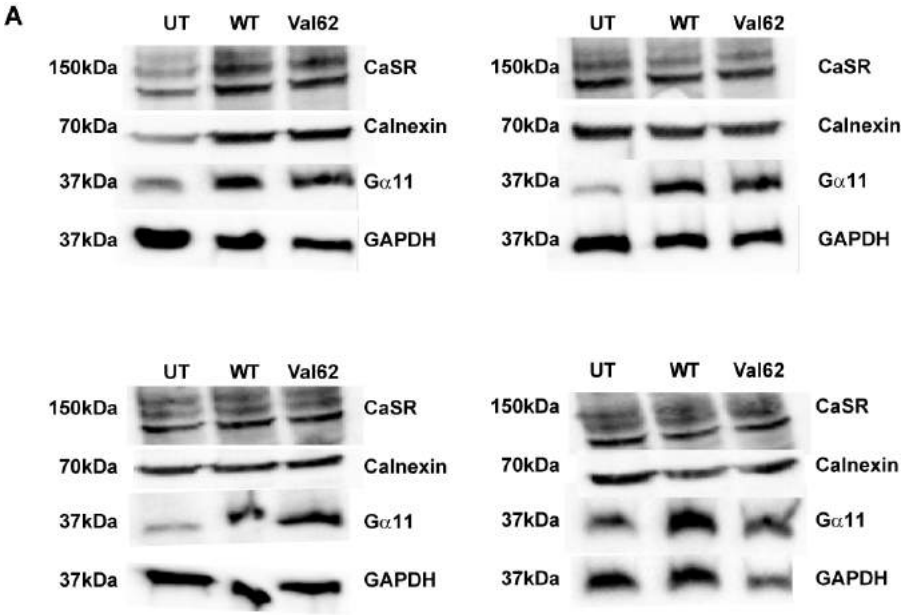

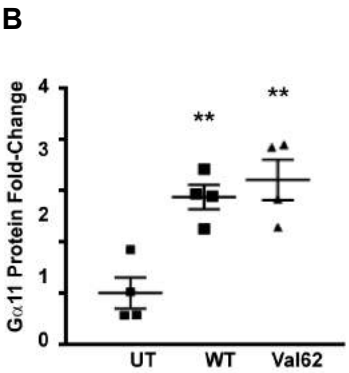

Supplementary Figure 2. Cells transiently transfected with WT and mutant Val62 pBI-CMV2-*GNA11* constructs overexpress the Ga_{11} protein. (A) Four separate Western blots of lysates from HEK-CaSR cells transiently expressing WT (Ile62) or mutant (Val62) pBI-CMV2-*GNA11* constructs. Transient transfection with WT or mutant Val62 expression constructs resulted in overexpression of $G\alpha_{11}$ compared to untransfected cells (UT). GAPDH was used as a housekeeping protein for $G\alpha_{11}$ blots, and calnexin for CaSR blots. (B) Densitometric analysis of $G\alpha_{11}$ protein levels in each of the blots. $G\alpha_{11}$ expression was normalized to levels of GAPDH and expressed as a fold-change of $G\alpha_{11}$ expression in UT cells. $G\alpha_{11}$ was significantly overexpressed in transfected cells compared to UT cells. The expression of mutant $G\alpha_{11}$ with endogenous WT $G\alpha_{11}$ in transfected cells corresponded to the heterozygous situation *in vivo*. Data is expressed as mean±SEM of the 4 blots which represent 4 independent lysates. Statistical analyses were performed using two-way ANOVA. **P<0.01.

Supplementary Figure 3

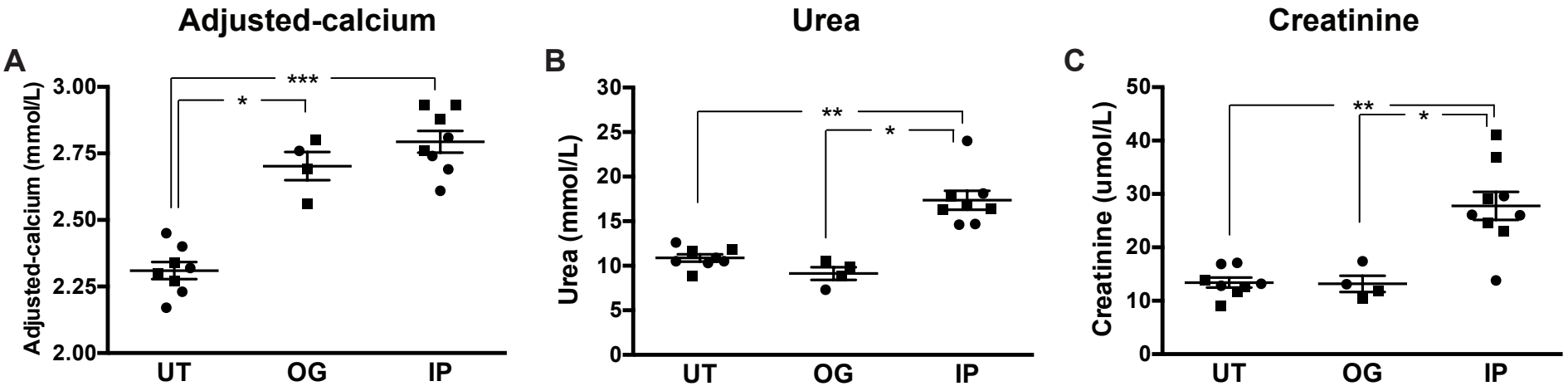

Supplementary Figure 3. Comparsion of route of administration of NPS-2143 on plasma calcium and renal function in WT mice. (**A**) plasma adjusted-calcium, (**B**) plasma urea, and (**C**) plasma creatinine concentrations of untreated (UT) WT mice, and of WT mice given NPS-2143 by oral gavage (OG) or intraperitoneal (IP) injection. Plasma biochemistry was measured at 1hr post-dose in NPS-2143-treated mice. Mean±SEM values for the respective groups are indicated by solid bars. Squares, males; circles, females. *P < 0·05,**P < 0·01, ***P < 0.001. A Kruskal-Wallis test followed by Dunn's test for non-parametric pairwise multiple comparisons were used for analysis of A-C.

Supplementary Figure 4

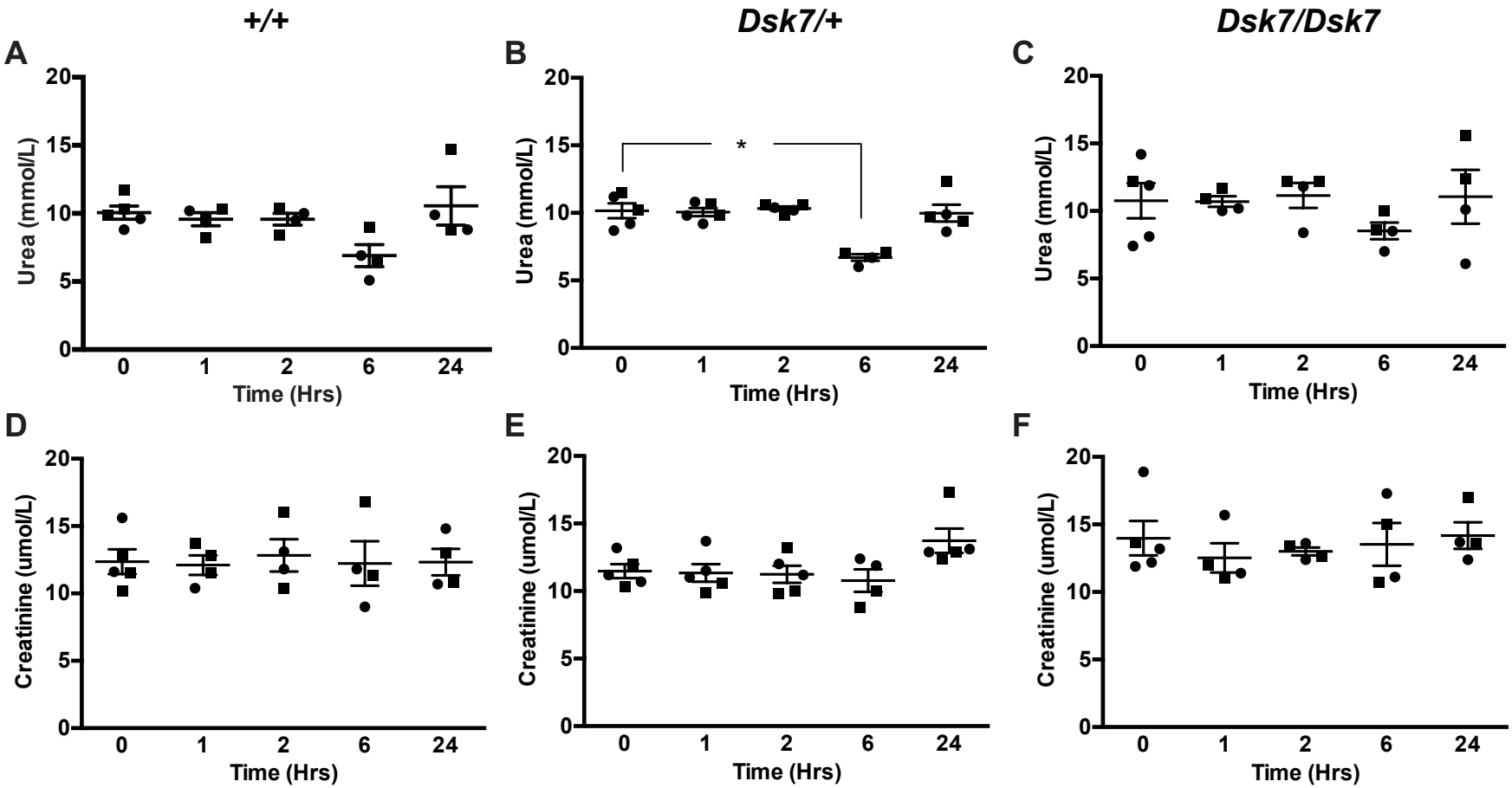

Supplementary Figure 4. Effect of NPS-2143 on plasma urea and creatinine of WT and Dsk7 mice at 0, 1, 2, 6 and 24hrs post-dose. (**A-C**) plasma urea and (**D-F**) plasma creatinine concentrations of WT (+/+), Dsk7/+ and Dsk7/Dsk7 mice, respectively. Mean±SEM values for the respective groups are indicated by solid bars. N=4-5 mice per study time-point. Squares, males; circles, females. *P < 0.05. A Kruskal-Wallis test followed by Dunn's test for non-parametric pairwise multiple comparisons were used for analysis of A-F.

Supplementary Figure 5

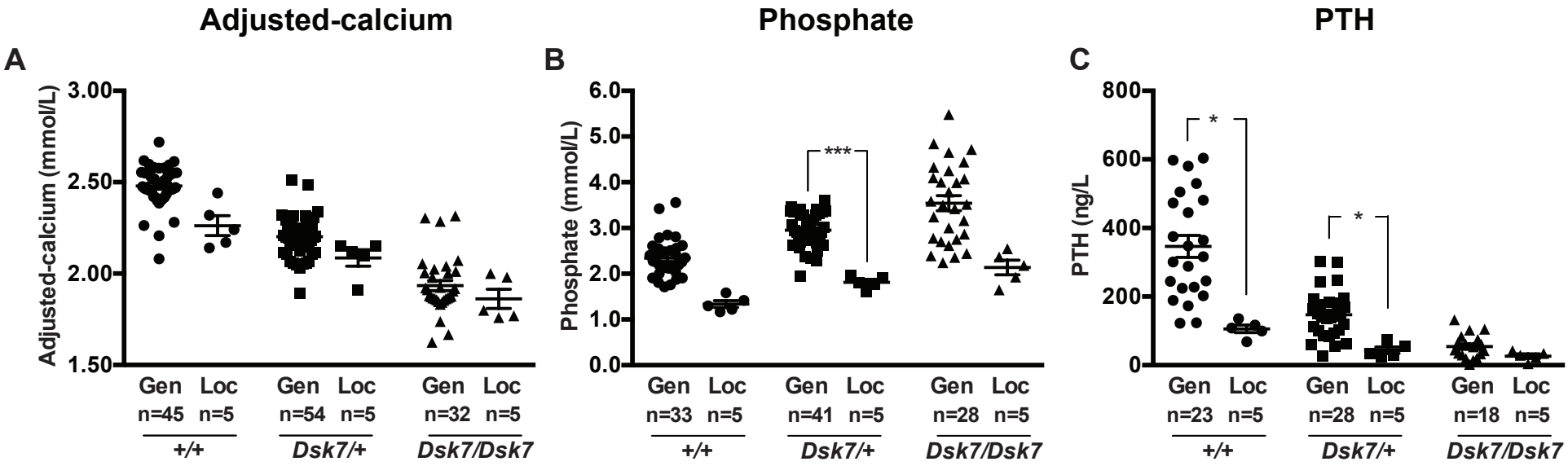

Supplementary Figure 5. Comparsion of effect of isoflurane general anesthesia versus topical local anesthesia on plasma concentrations of calcium, phosphate and PTH. (**A**) plasma adjusted-calcium, (**B**) plasma phosphate, and (**C**) plasma PTH concentrations of +/+ (WT), Dsk7/+ and Dsk7/Dsk7 mice. Mean±SEM values for the respective groups are indicated by solid bars. Circles, +/+ mice; squares, Dsk7/+ mice; triangles, Dsk7/Dsk7 mice. Gen, general isoflurane anesthesia; Loc, local anesthesia.*P < 0·05, ***P < 0.001. A Kruskal-Wallis test followed by Dunn's test for non-parametric pairwise multiple comparisons were used for analysis of A-C.